Integrated Multi-Mission Ocean Altimeter Data for Climate Research TOPEX/Poseidon, Jason-1, 2, & 3, Sentinel-6a User's Handbook Version 6.0

Brian Beckley	ERT, Inc.
Richard Ray	NASA/Goddard Space Flight Center
Nikita Zelensky	University of Maryland
Frank Lemoine	NASA/ Goddard Space Flight Center
Xu Yang	KBR Inc.
Josh Willis	Jet Propulsion Laboratory/California Institute of Technology
Severine Fournier	Jet Propulsion Laboratory/California Institute of Technology
Emmy Killett	Jet Propulsion Laboratory/California Institute of Technology
Kevin Marlis	Jet Propulsion Laboratory/California Institute of Technology
Celia Ou	Jet Propulsion Laboratory/California Institute of Technology
Shannon Brown	Jet Propulsion Laboratory/California Institute of Technology
Shailen Desai	Jet Propulsion Laboratory/California Institute of Technology
Gary Mitchum	University of South Florida

Table of Contents

Table of Figures

Introduction

Maintenance and improvements to the fidelity of the TOPEX/Poseidon, Jason-1, Jason-2/OSTM, Jason-3, and Sentinel-6a Sea Surface Height (SSH)Climate Data Record (NASA-SSH) is a continuous effort through the research activities of the Ocean Surface Topography Science Team (OSTST). As further advancements and/or re-calibrations are made to any of the correction parameters or models, the along-track SSH product is recalculated with the most accurate algorithms sanctioned by the OSTST. Notification and details of revisions to the TPJAOS will be provided and announced by the Physical Oceanography Distributed Active Archive Center (PODAAC) and displayed at this site http://podaac.jpl.nasa.gov/Integrated_Multi-Mission_Ocean_AltimeterData. Users will be notified of revisions to ensure they are consistently up to date.

In summary the following revisions were incorporated in the development of the NASA-SSH (formerly MEaSUREs) along-track sea surface height anomaly product:

Several algorithm revision/improvements along with the integration of Jason-3 data prompted the release of a revised version 4.0 in March of 2017. GSFC itrf2014/dpod4-based orbit replacing std1504 for all missions

- Extending SSH time series with Jason-3 altimetry
- DTU15 MSS reference
- Cross-track gradient correction based on DTU15 MSS derived cross-track slopes
- Revised inter-mission bias estimates

A minor revision (v4.1) was implemented to reprocess the orbits for a few Jason-3 cycles with improved DORIS tracking. The version 4.2 update involved the removal of the TOPEX cal-1 mode range correction (Beckley et al., 2017) and the subsequent inter-mission bias revisions. Version 5.0 sea surface heights are with respect to revised GSFC std2006 orbit standards, and Version 5.1 implemented Jason-3 GDR_F standards to several geophysical corrections. The last version, Version 5.2, contained the following revisions to v5.1:

- GSFC std2006_cs21 orbit for all missions
- GOT5.1 ocean tide model
- TOPEX/Poseidon GDR_F data
- Sentinel-6 LR version F08 data
- Jason-3 re-calibrated radiometer wet troposphere correction

The current Version 6.0 contains the following revisions to v5.2:

- GSFC std2400 orbit for T/P and Jason-1 (cycles 169 – 259)
- JPL_igs20 orbit for Jason-1 (cycles 1 – 168), Jason-2, Jason-3, and Sentinel-6a
- ITRF2020 terrestrial reference frame
- Jason-2 GDR_F data
- Sentinel-6a LR version F09/G01 data through cycle 166
- GOT5.6D ocean tide model
- Range latitudinal empirical correction for Jason-1,2, & 3 GDRs

The following sections of this report detail these previous and more current revisions to the SSH record, and any subsequent impacts to validation results and mean sea level estimates.

1.0 General Structure Characteristics

The NASA-SSH v6.0 sea surface height (SSH) anomaly product is a multi-mission data set comprised of TOPEX/Poseidon (T/P), Jason-1, OSTM (Jason-2), Jason-3, and Sentinel-6a altimeter data integrated to form a single SSH Climate Data Record (CDR). Altimeter data from the multi-mission Geophysical Data Records (GDRs) are interpolated to a common reference orbit facilitating direct time series analysis of the geo-referenced SSH. The baseline v6.0 merged file is comprised of 1,203 10-day repeat cycles:

Cycle	001 – 360	T/P (cycles 1 – 360)
	361 – 582	Jason-1 (cycles 18 -239)
	583 – 865	Jason-2 (cycles 1 – 283)
	866 – 1,087	Jason-3 (cycles 4 - 225)
	1,088-1,203	Sentinel-6a (cycles 51 – 166)

As future Sentinel-6a cycles become available the direct access structure of the file allows new data to be appended. All inter-mission biases have been applied to provide a seamless transition throughout the current 30+ year record.

Each 10-day repeat cycle is comprised of 127 revolutions. Each revolution has 6745 along-track locations spanning the equatorial ascending node (Figure 1).

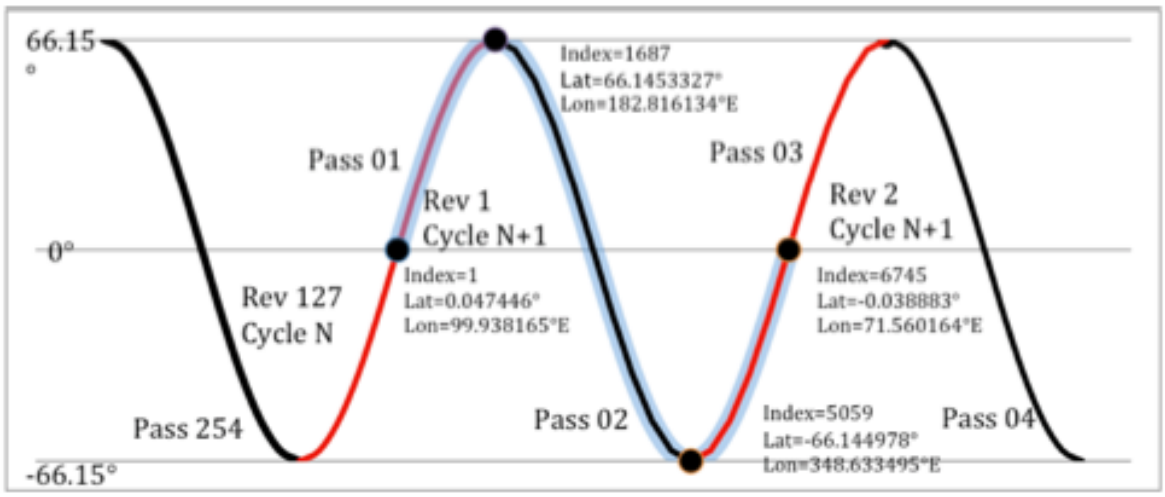

Figure 1: ***GDR convention of ascending odd numbered passes (solid red lines) and descending even numbered passes (solid black lines) total 254 passes/repeat cycle. The NASA-SSH (formerly NASA MEaSURE's) product convention is based on 127-revolutions/repeat cycle. Revolution #1 is shown (blue shading overlay) with reference orbit lat/lon coordinates indicated for first and last geo-reference index, and for index at maximum and minimum latitude.***

Each SSH data record is a SSH time series at a specific geo-referenced location defined by revolution number and along-track index. A 3-dimensional directory (rev#, index, cycle) permits direct access of individual locations at specific times (i.e. temporal and spatial sub-sampling). Auxiliary files provide time, mean sea surface reference, terrain type, bathymetry, proximity to coast, and SSH quality assessments (flag word) at each geo-referenced location.

1.1 Geo-referenced 1Hz SSH

Construction of the 1Hz geo-referenced SSH is achieved by sampling the 20Hz GDR high-rate SSH from contiguous 1Hz samples that align with the reference index location, and the time at the reference location derived from the GDR (Figure 2).

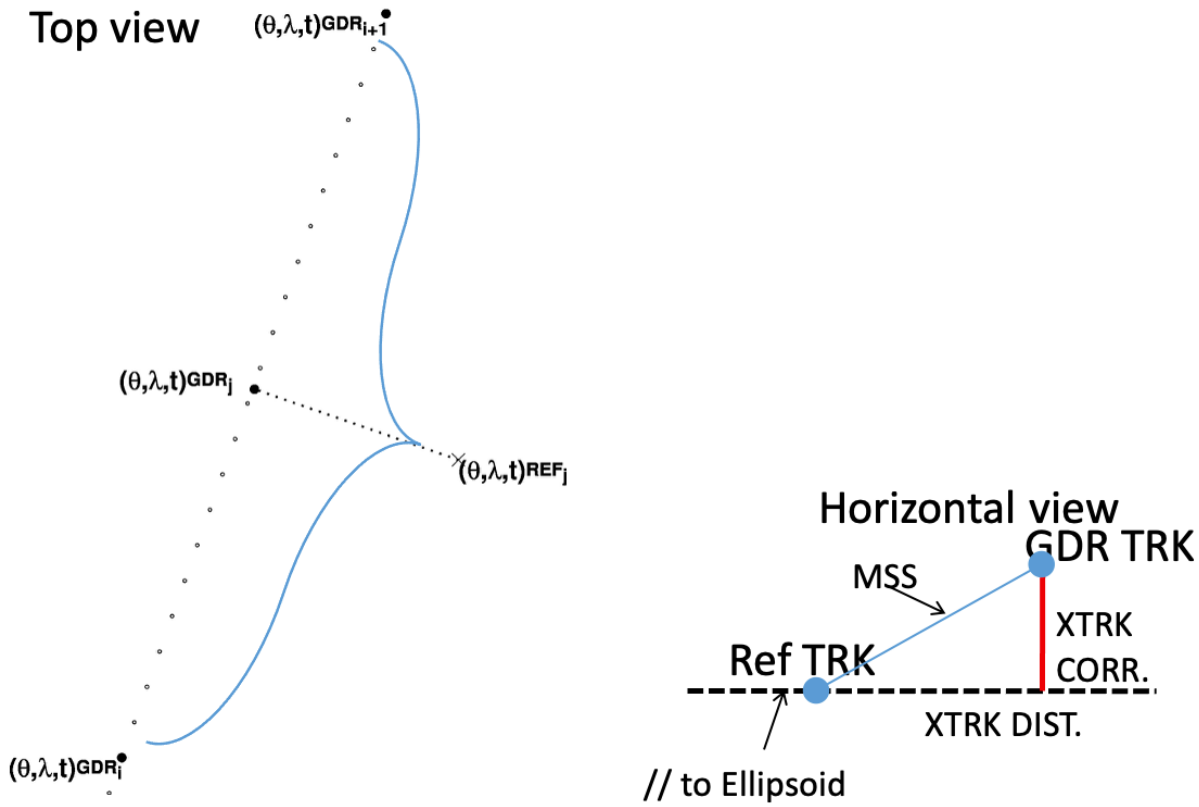

Figure 2: ***1Hz SSH constructed at reference orbit locations (REF $_j$) is achieved by re-sampling high-rate SSH from contiguous 1Hz GDR SSH (GDR $_i$ and GDR $_{i+1}$) evaluated at mid-point GDR $_j$.***

Satellites can deviate from the nominal orbit ground track by up to ± 1 km. To correct for this, a Mean Sea Surface [MSS] model can be used to effect a cross-track transformation between the along-track SSH and the corresponding SSH on the reference orbit. Towards this end, the normal projected onto the GDR groundtrack from the reference location provides the cross-track distance. The product of the cross-track distance and the local slope of the DTU15 MSS (Andersen et al., 2015) provide the cross-track gradient correction (Brenner et al, 1990) applied to account for local MSS gradients. The regression fit of the high-rate SSH is performed employing the GDR routine g1071 (TOPEX Ground System Science Algorithm Specification, 1991). Additional constraints require a minimum number of high-rate SSH , and a minimum number of high-rate SSH on each side of the midpoint . The standard deviation of the high-rate residuals with respect to the resultant

1Hz average fit is computed and incorporated in the SSH quality assessment flag word (see Table 2).

1.2 Construction of the Corrected SSH Anomaly

$SSH_{uncorrected}$ = Orbit (GSFC std2400/JPL_igs20) – $Range\_ku_{corrected\ (net\_instrument\_corection\_ku)}$
$SSH_{corrected}$ = $SSH_{uncorrected}$ - Dry Troposphere Delay
- Wet Troposphere Delay
- Solid Earth Tide
- Ocean Tide
- Ocean Load Tide
- Long-Period Tide
- Internal Tide
- Pole Tide
- Ionosphere Delay
- Sea State Bias (SSB) Delay
- Dynamic Atmospheric Correction (DAC)
- Cross-track gradient
+ inter-mission bias

$SSH_{anomaly}$ = $SSH_{corrected}$ - DTU15 mean sea surface

Note: The SSH anomalies are with respect to DTU15 MSS. The user can construct SSH anomalies with respect to a collinear mean reference by first adding back the DTU15 MSS, which is made available as a separate auxiliary file.

The version 6.0 GDR heritage for each mission:

- T/P GDR_F (TOPEX/POSEIDON GDR_F Handbook, CNES Reference: SALP-MU-MAO-OP-17607-CN, JPL Reference: JPL D-73899, Issue: 1 rev 0, June 16, 2023)
- Jason-1 GDR_E (Picot et al., 2016)
- OSTM GDR_F (OSTM/Jason-2 products handbook, April, 2025)
- Jason-3 GDR_F (Jason-3 Products handbook, September 2020)
- Sentinel-6a F09/G01 (Along-track Level-2+ (L2P) Sea Level Anomaly Sentinel-3 / Jason-CS-Sentinel-6 Product Handbook, Nomenclature: SALP-MU-P-EA-23014-CLS, Issue: 3 rev 3, November 2022); Sentinel-6 altimetry level 2 and 3 data guide, V1.2, 7 Aug 2025.

Origination of individual range and geophysical corrections applied to the SSH for each mission is detailed in Table 1. Corrections employed that were directly obtained from GDR are identified by their parameter name as in handbook in bold italics. Some of the altimeter corrections present on the mission GDRs have been recomputed to take advantage of more recent and accurate models and to insure consistency across missions. The development

and implementation of replacement or revised correction parameters are explained in sections below.

	TOPEX	Poseidon-1	Jason-1	Jason-2 (OSTM)	Jason-3	Sentinel-6a
Orbit	GSFC std2400 referenced to ITRF2020	GSFC std2400 referenced to ITRF2020	Cycles 001 - 168 JPL_igs20 Cycles 169-259 GSFC std2400 referenced to ITRF2020	JPL_igs20 referenced to ITRF2020	JPL_igs20 referenced to ITRF2020	JPL_igs20 referenced to ITRF2020
Range Ku	MLE4 ***range_20hz_ku***	MLE4 ***range_ku***	MLE4 ***range_ku_20hz***	MLE4 ***range_ocean_20hz_ku ****	MLE4 ***range_ocean_20hz_ku***	Numerical retracker ***range_ocean_nr_20hz_ku***
Dry Trop.	**model_dry_tropo_cor_zero_altitude**	**model_dry_tropo_cor_zero_altitude**	***model_dry_tropo_corr***	***model_dry_tropo_cor_zero_altitude_1hz***	***model_dry_tropo_cor_zero_altitude_1hz***	***model_dry_tropo_cor_zero_altitude_1hz***
Wet Trop.	GDR_F TMR ***rad_wet_tropo_cor***	GDR_F TMR ***rad_wet_tropo_cor***	GDR_E JMR ***rad_wet_tropo_corr***	GDR_F AMR ***rad_wet_tropo_cor_1hz***	GDR_F AMR ***rad_wet_tropo_corr*****	F09/G01 LR ***rad_wet_tropo_corr***
Ocean Tide	GOT5.6D	GOT5.6D	GOT5.6D	GOT5.6D	GOT5.6D	GOT5.6D
Ocean Load Tide	GOT5.6	GOT5.6	GOT5.6	GOT5.6	GOT5.6	GOT5.6
Long-Period Tide	Ray & Erofeeva (2014)	Ray & Erofeeva (2014)	Ray & Erofeeva (2014)	Ray & Erofeeva (2014)	Ray & Erofeeva (2014)	Ray & Erofeeva (2014)
Internal Tide	Zaron (2019) V8.1	Zaron (2019) V8.1	Zaron (2019) V8.1	Zaron (2019) V8.1	Zaron (2019) V8.1	Zaron (2019) V8.1
Pole Tide	Desai et al., 2015; Ries and Desai 2017 (v2.2)	Desai et al., 2015; Ries and Desai 2017 (v2.2)	Desai et al., 2015; Ries and Desai 2017 (v2.2)	Desai et al., 2015; Ries and Desai 2017 (v2.2)	Desai et al., 2015; Ries and Desai 2017 (v2.2)	Desai et al., 2015; Ries and Desai 2017 (v2.2)
Solid Earth Tide	***solid_earth_tide***	***solid_earth_tide***	***solid_earth_tide***	***solid_earth_tide_1hz***	***solid_earth_tide***	***solid_earth_tide***
Iono	Dual-frequency **iono_cor_alt_ku** ***(smoothed)***	Doris/GIM ***Iono_Dor Iono_cor_gim_ku***	Dual-frequency ***iono_corr_alt_ku (smoothed)***	Dual-frequency ***iono_cor_alt_1hz_ku (smoothed)***	Dual-frequency ***iono_corr_alt_ku (smoothed)***	Dual-frequency ***iono_corr_alt_nr_1hz (smoothed)***
Sea State Bias	Non-parametric ***sea_state_bias_ku***	***sea_state_bias_ku***	Non-parametric collinear residuals (Tran et. al, 2012) ***sea_state_bias_ku***	Non-parametric collinear residuals ***sea_state_bias_1hz_ku***	Non-parametric collinear residuals (Tran et al 2020) ***sea_state_bias_ku***	Non-parametric collinear residuals ***sea_state_bias_nr_ku***
Atmos-pheric load	Dynamic Atmospheric Correction (***dac***)	Dynamic Atmospheric Correction (***dac***)	ECMWF ERA-interim + MOG2D hi-frequency ***inv_bar_corr + hf_fluctuations corr***	Dynamic Atmospheric Correction ***dac***	Dynamic Atmospheric Correction ***dac***	Dynamic Atmospheric Correction ***dac***

Cross-Track gradient	DTU15 MSS	DTU15 MSS	DTU15 MSS	DTU15 MSS	DTU15 MSS	DTU15 MSS
Inter-mission bias wrt Jason-2	A1: -36.4 mm A2: -40.9 mm B: -4.2 mm	adjusted to adjacent TOPEX cycles (see Figure (17)	Cycles 1-168: -0.42 mm Cycles 169-259: -1.35 mm	0.0 mm	32.0 mm	26.7 mm

*Range latitudinal empirical correction applied for Jason-1, 2, & 3 (Cadier et al., 2024)
**Jason-3 radiometer recalibration range bias correction applied (Brown et al., 2023).

Table 1: Heritage of range and geophysical corrections applied to the SSH for each mission.

A SSH anomaly with respect to the DTU15 mean sea surface (Andersen, 2016) is computed if all correction fields are available (i.e. various conventions used throughout not set to default value). If one or more of the corrections applied are outside accepted nominal ranges, a quality assessment flag word bit is set to indicate the less-than-optimal quality. This rationale allows maximum retention of coastal and inland water observations that may otherwise be edited as "blunders" by open ocean standards. Table 2 lists the nominal ranges for each correction that with few exceptions follows the GDR handbook recommendations.

Table 2: Nominal ranges for individual correction parameters. Quality flag word bit #6 (see SSH Quality Flag Word description below) is set if any single correction parameter is outside nominal range.

Correction parameter	Nominal range
Dry Troposphere	> -2600 mm and < -1900 mm
Wet Troposphere	≥ -600 mm and < 0 mm
Ocean Tide	> -5 m and < + 5 m
Load Tide	> -150 mm and < +150 mm
Pole Tide	≥ -100 mm and ≤ +100 mm
Solid Earth Tide	≥ -1000 mm and ≤ +1000 mm
Sea State Bias	≥ -600 mm and ≤ 0 mm
Altimeter derived wind speed	≥ 0 m/s and < 25 m/s
Atmospheric load	≥ -1000 mm and ≤ +1000 mm

1.3 SSH Quality Flag Word

For each 1Hz geo-referenced SSH anomaly, a flag word is assigned to further assess the quality of the resultant SSH determination and provide the capability for tailored edit strategies for particular user applications.

Bit 0: blank

Bit 1: = 0 Dual-frequency altimeter measurement and JPL_igs20 orbit
= 1 Single frequency altimeter measurement and/or GSFC std2400 orbit

Bit 2: = 0 depth ≥ 200 meters
= 1 depth < 200 meters

Bit 3: = 0 proximity to land ≥ 50 km
= 1 proximity to land < 50 km

Bit 4: = 0 Sigma H of fit < 15 cm (< 20 cm for Poseidon-1)
= 1 Sigma H of fit ≥ 15 cm (≥ 20 cm for Poseidon-1)

Bit 5: = 0 high rate SSH sampled from two contiguous 1Hz data observations
= 1 high rate SSH sampled from single 1Hz observation

Bit 6: = 0 all SSH corrections within nominal range
= 1 one or more of SSH corrections outside nominal range

Bit 7: = 0 Cross Track Distance < 1.0 km.
= 1 Cross Track Distance ≥ 1.0 km.

Bit 8: = 0 Cross Track Slope < 10 cm/km.
= 1 Cross Track Slope ≥ 10 cm/km.

Bit 9: = 0 Significant Wave Height < 8 m and > 0 m (Ku band)
= 1 Significant Wave Height ≥ 8 m or = 0 m (Ku band)

Bit 10: = 0 Sea ice not detected
= 1 Sea ice detected

Bit 11: = 0 No rain contamination detected
= 1 Possible rain contamination detected.

Bit 12: = 0 Sigma0 ≥ 6 db and ≤ 27 db (Ku band)
= 1 Sigma0 < 6 db or > 27 db (Ku band)

Bit 13: = 0 Attitude (Att_Wvf) ≥ 0 and ≤ 0.3 degrees (T/P)
= 0 off_nadir_angle_ku_wvf ≥ -.09 deg^2 and ≤ +.09 deg^2
= 1 Attitude (Att_Wvf) < 0 or > 0.3 degrees (T/P)
= 1 off_nadir_angle_ku_wvf < -.09 deg^2 or > +.09 deg^2

Bit 14: = 0 radiometer observation NOT suspect (tmr_bad set=0)
= 1 radiometer observation suspect (tmr_bad set > 0)

Bit 15: = 0 ABS (SSH (cycle N)-SSH (cycle N-1)) < 50 cm
or ABS (SSH (cycle N)-SSH (cycle N-1)) < 50 cm
= 1 ABS (SSH (cycle N)-SSH (cycle N-1)) > 50 cm
and ABS (SSH (cycle N)-SSH (cycle N-1)) > 50 cm

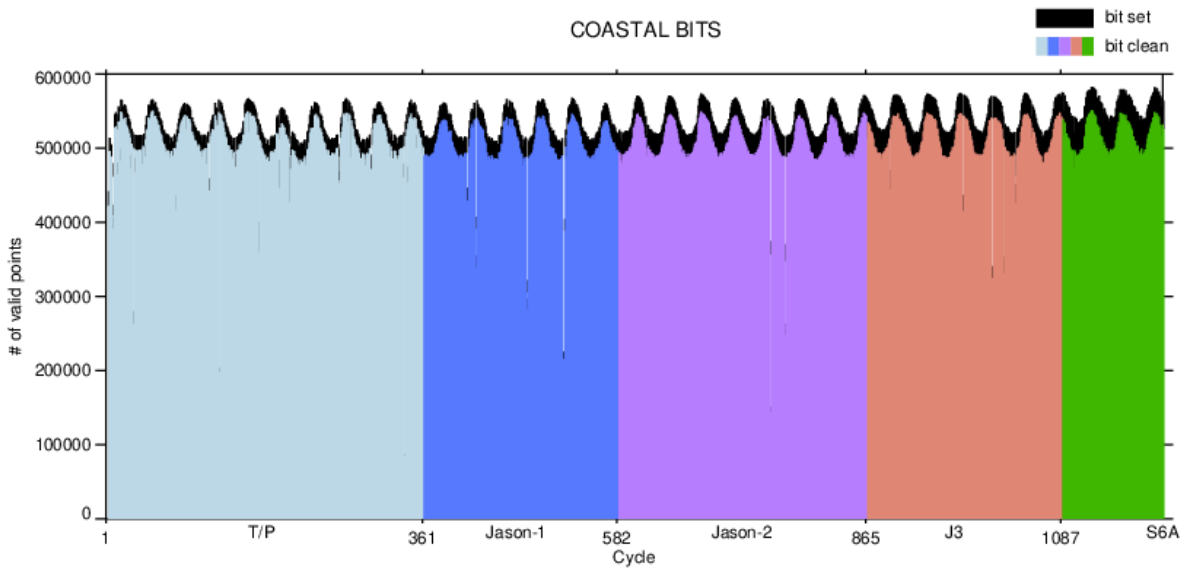

Figure 3: ***Approximately 5% of valid (not set to default value of 32767) open ocean SSH anomalies are edited based on an edit strategy that requires bits 4-14 pass (i.e. equal 0) bits 1-3 and 15 are not checked thus retaining Poseidon-1 and coastal observations.***

2.0 Version 6.0 addendum revisions to SSH computation

2.1 The GSFC std2400 and JPL_igs20 replacement orbit height correction

Accurate orbit determination is central to the computation of the altimeter-derived surface elevation observation. The orbit defines the geocentric reference for the satellite altimeter sea surface measurement. Orbit accuracy and consistency are essential not only to the altimeter measurement accuracy across one mission, but also for the seamless transition between missions (Beckley, et. al, 2004). The analysis of altimeter data for TOPEX/Poseidon (TP), Jason-1 (J1), Jason-2 (J2), Jason-3 (J3), and Sentinel-6a (S6A) requires that the orbits for all five missions be in a consistent reference frame, and calculated with the best possible standards to minimize error and maximize the data return from the time series, particularly with respect to the demanding application of consistently measuring global sea level change.

Ensuring the highest accuracy and consistency of the satellite orbit is a critical component facilitating accurate GMSL estimates. Foremost is the application of improved GSFC replacement orbits that would tie multiple missions to a common well-defined geodetic reference frame (Beckley et al., 2007) and gravity field (Lemoine et al., 2010). Orbit testing at GSFC, has shown progressive improvement with increasingly refined POD modeling. Since 2009 GSFC has released seven orbit series based on progressively improved POD standards: 1) the ITRF2005-based std0905, 2) the ITRF2008-based std1007 used previously in the MEaSURE's v1.0 product, 3) std1204 standards implemented in the MEaSURE's v2.0 product, 4) the ITRF2008-based std1504 standards implemented in the MEaSURE's v3.0 product, 5) the ITRF2014-based dpod2014 standards (Zelensky et al., 2017) implemented in the MEaSURE's v4.0 and v4.2 product, 6) the ITRF2014-based std2006 standards implemented in the MEaSURE's v5.0 and v5.1 product, including the std2006_cs21 (std2006_cs21 differs from std2006 only in a better modelling of the C21/S21 gravity coefficients) MEaSURE's v5.2 orbit , and now 7) std2400 referenced to ITRF2020 (Alatamimi et al., 2023).

For v6.0 a "hybrid" combination of GSFC std2400 + JPL jpl_igs20 orbits are implemented to generate the 32+ year SSH along-track time series. This "hybrid" combination contains the std2400 orbit where the GPS-based jpl_igs20 orbits are not available, that is over TOPEX, Jason-1 cycles 169-259 (August 2006 – January 2009), and wherever there are gaps in the jpl_igs20 time series over the remaining missions. The rationale is that a "hybrid" orbit time series would take advantage of the best-available orbits for each particular satellite in order to compute a global mean sea level estimate. The current GSFC replacement orbits, std2400, are dynamic orbits based on Satellite Laser Ranging (SLRF2020) and DORIS (DPOD2020) data, improved background gravity modelling, improved non-conservative force modelling, and application of the GOT5.6 ocean tide model (Lemoine et al., 2025). The JPL_igs20 orbits are reduced-dynamic and are based on GPS tracking only (Bertiger et al., 2010, Conrad et al., 2023, 2024). The direct impact on GMSL estimates between the v6.0 GSFC std2400 + JPL jpl_igs20 orbits and the v5.2 GSFC std2006_cs21 is shown in Figure 4. The significant difference at the end of the time series is explained in Figure 5 as primarily due to differences in the time variable gravity (TVG) modeling (see Rudenko et al., 2014), and the transition to ITRF2020.

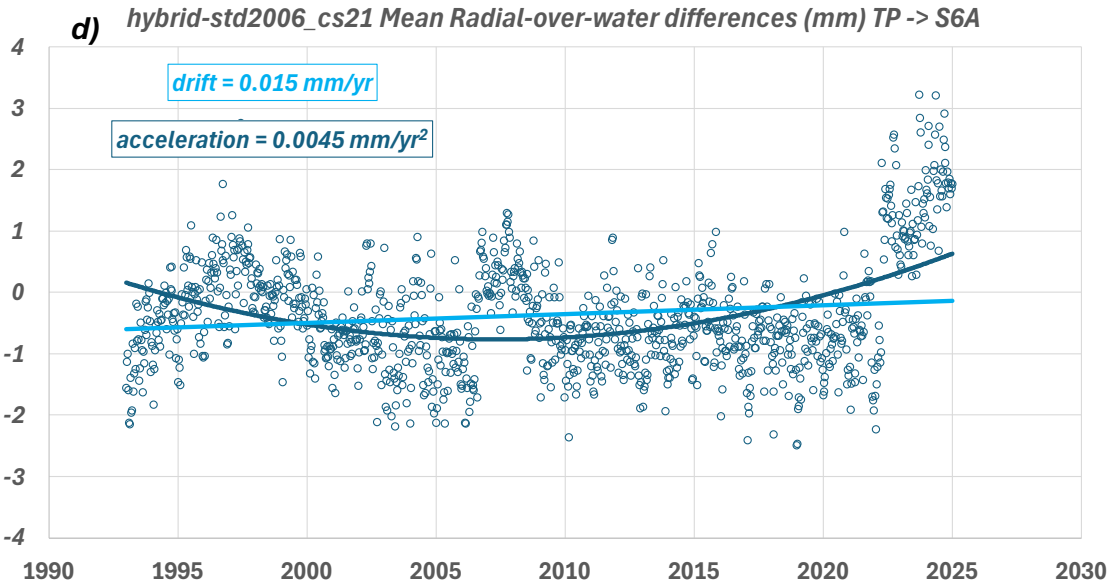

Figure 4: ***Radial orbit differences over water rate and acceleration terms from 1993.0 to 2025.0 computed for (d) hybrid (jpl_igs20/std2400) – std2006_cs21 (Figure 10d from Lemoine et al., 2025).***

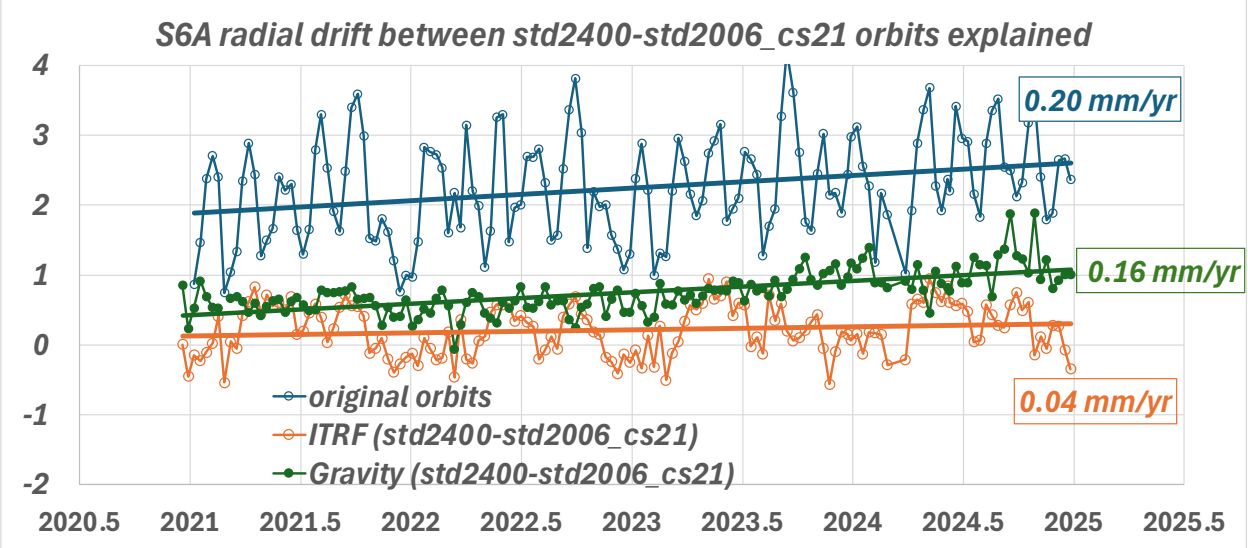

Figure 5: ***Sentinel-6A radial orbit drift computed using 10-day mean radial differences over water, over 4-years (cycles 4-152). The 0.20 mm/yr drift between the std2400 – std2006_cs21 orbits (blue) is explained by the 0.16 mm/yr drift between the (std2400) COSTG_FSM+SLR and the (std2006_cs21) GSFC TVG models (green), plus the 0.04 mm/yr drift between the ITRF2020-ITRF2014 orbits (orange) (Figure 5 from Lemoine et al., 2025).***

2.1 Re-calibrated Jason-1 and Jason-3 Microwave Radiometers

Over the course of the Jason-1 mission several re-calibrations were performed to maintain and adhere to wet path delay (PD) stability/drift requirements (Brown, 2014). The most recent re-calibration is the end-of-mission climate quality calibration for the JMR (Brown, 2014) included in the GDR_E release. The end-of-mission re-calibration builds on previous calibrations, addresses remaining short term and long-term residual calibration instability issues evident in the data (Figure 6), and implements revised algorithms brought up to Jason-2 GDR_D standards.
To stabilize the long-term calibration, an inter-satellite calibration approach was applied. This approach essentially transfers the long-term calibration from other stable externally calibrated satellite microwave radiometers to the altimeter radiometers. The calibration standard in this case was chosen to be the SSM/I TB fundamental climate data record (FCDR) (Kummerow et al., 2010).

In addition to the long-term trend, JMR also exhibited time variable changes in calibration instrument temperature dependency. The effect is to introduce transient 60-day variations, which cannot be easily detected using the TB references, but is very apparent when comparing the geophysical retrievals to other references. A process was developed to infer the TB instrument temperature dependence over a 120-day moving window from comparisons of the path delay to the ECMWF model and the AMR wind speed to the altimeter wind speed. This correction was applied along with the long-term drift.
Finally, the JMR algorithms were updated to the Jason-2 GDR-D standard using the same processing software as is used for Jason-2 processing, but with coefficients specific to the JMR.
A drift correction has been applied to the final GDR_C calibration, which takes the form of a time variable scale and offset correction:

$$TB(ch,t)_{corrected} = TB(ch,t)_{uncorrected} - \Delta T_B(ch,t)$$

$$\Delta T_B(ch,t) = c_0(ch,t) + c_1(ch,t)TB(ch,t)_{uncorrected}$$

where the coefficients are derived by forcing agreement with the SSM/I Tb FCDR and on-Earth references (over the ocean (cold end) and over the Amazon rainforest (warm end)). The SSM/I FCDR was developed by Colorado State University (CSU) for NOAA and extends from 1987 to the present, covering the altimeter time period. The inter-satellite calibration provides a second independent reference (in addition to the natural reference method) and the demonstrated agreement between the two gives confidence in the observed long-term TB drift. Month-to-month calibration uncertainty is about 0.2°K (~2mm in PD). Estimated trend error (Figure 7) can be computed as a function of record length:

- 2 mm/yr uncertainty for any 1 year
- < 1 mm/yr uncertainty for time spans greater than 2 years
- << 1 mm/yr for mission

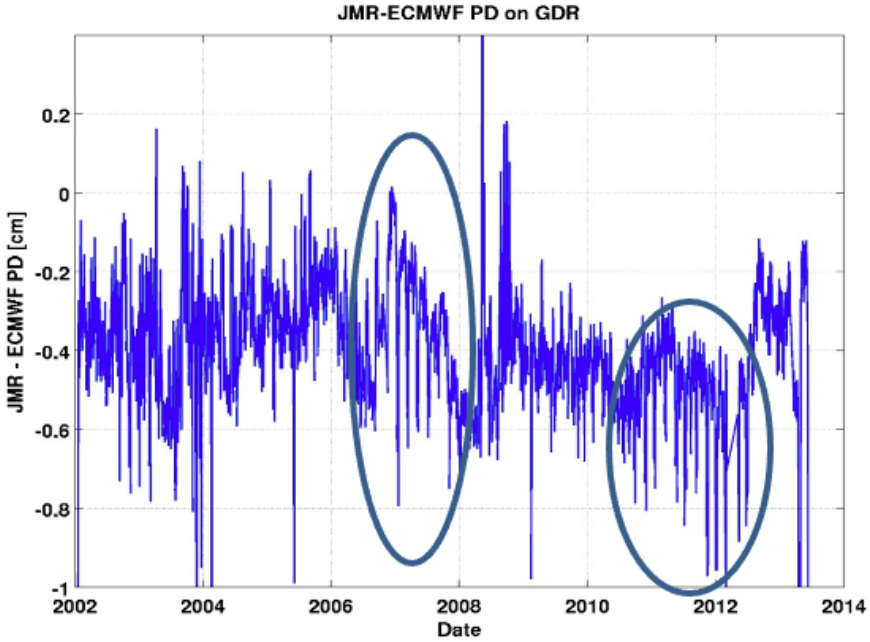

Figure 6: JMR (GDR_C) minus ECMWF mean path delay differences detect times where further re-calibration is warranted.

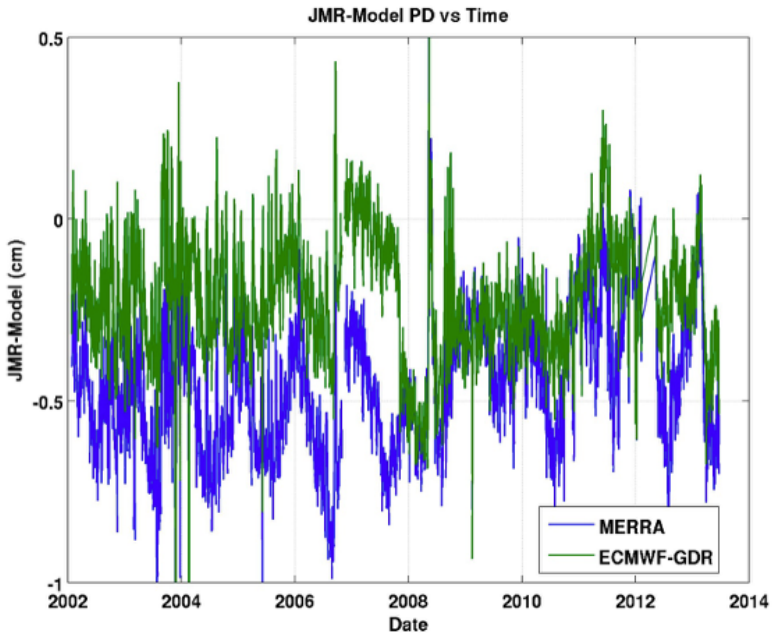

Figure 7: Re-calibrated JMR versus MERRA and ECMWF model wet path delays suggest JMR drift rate less than 1mm/decade.

Several JMR algorithms were updated to Jason-2 AMR standards:

- All-weather sigma-0 attenuation correction algorithm
- Consistent sea ice and rain flagging
- Near land path delay retrieval algorithm

A recent investigation of the Jason-3 AMR stability (Brown et al., 2023) revealed an approximate 2 mm/y drift in the wet troposphere path delay (Figure 8). A path delay correction (Figure 9) was applied to the Jason-3 GDR_F wet troposphere correction during the v5.2 and v6.0 SSH construction.

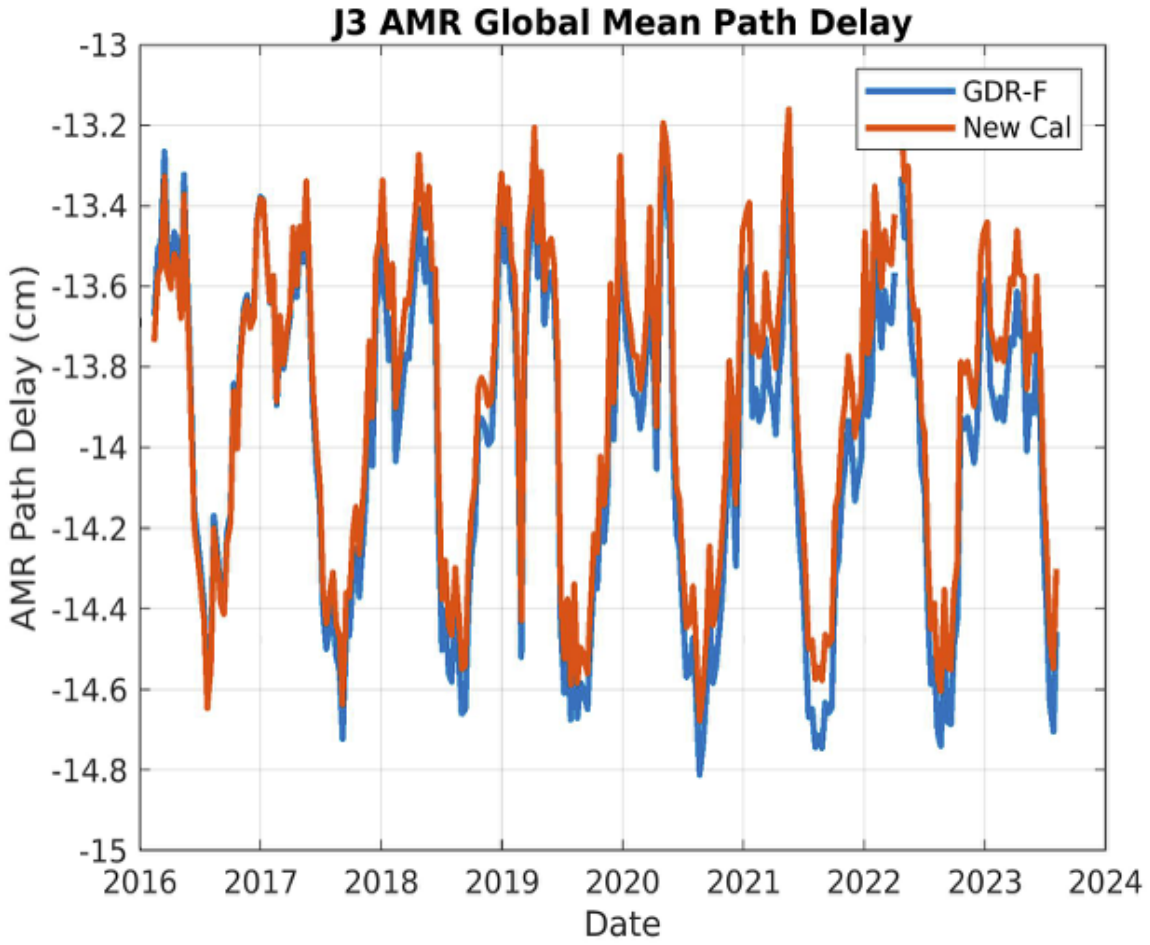

Figure 8: ***Jason-3 GDR_F AMR global mean path delay (blue line) compared to recalibrated AMR mean path delay (red line).***

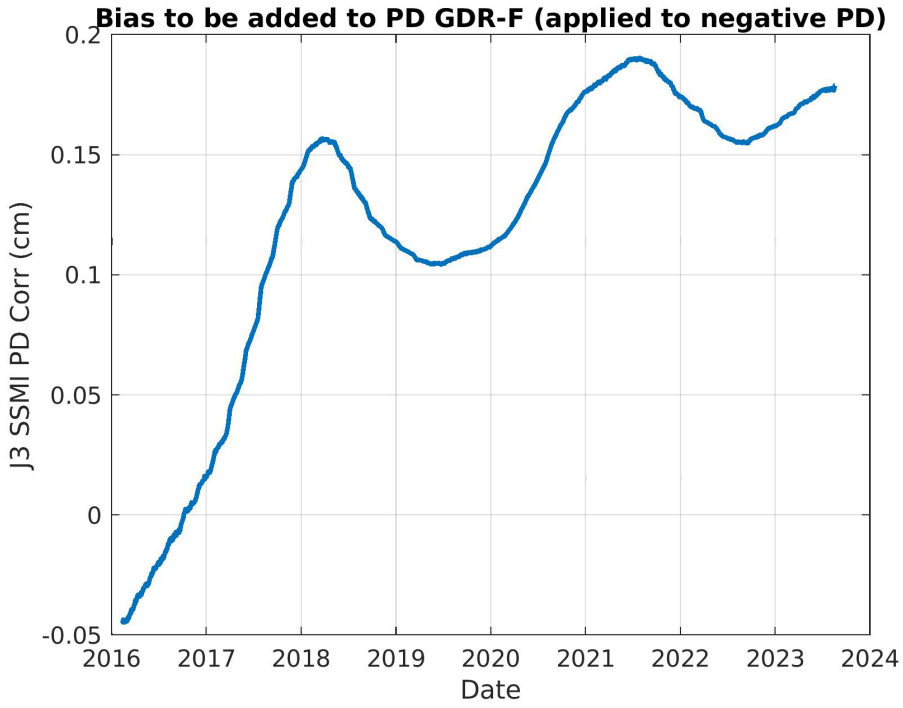

Figure 9: ***Bias applied to the Jason-3 GDR_F AMR wet troposphere path delay.***

2.3 TOPEX Microwave Radiometer (TMR) Enhanced Wet Path Delays

The wet tropospheric correction applied to the The initial GDR (MGDR_B) processing algorithm for TOPEX TMR uses a standard PD retrieval algorithm that underestimates path delay values near the coast due to land brightness temperature contamination. The application of a Mixed-Pixel algorithm Misra and Brown, 2011) non TOPEX TMR that has been successfully applied to the Advanced Microwave Radiometer (AMR) for Jason-2 and Jason-1 Microwave Radiometer (JMR) (Figure 10) to obtain coastal path delay values has been implemented. Algorithm performance on the TMR was compared with respect to the climate model MERRA (Figure 11) as well as JMR GDR processed PD values.

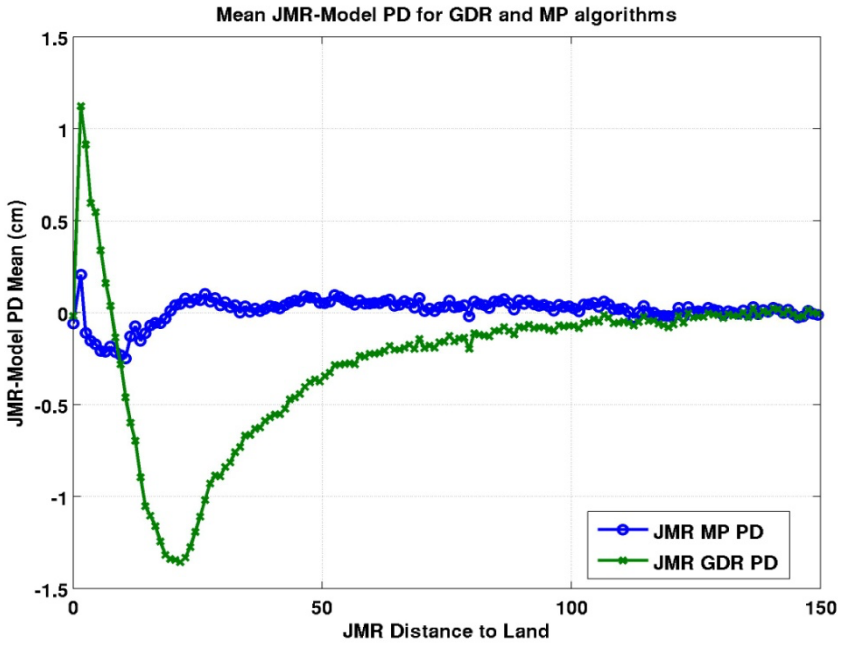

Figure 10: ***Enhanced GDR_E JMR path delays recovered near land via mixed pixel (MP) algorithms provide improved accuracies in coastal areas.***

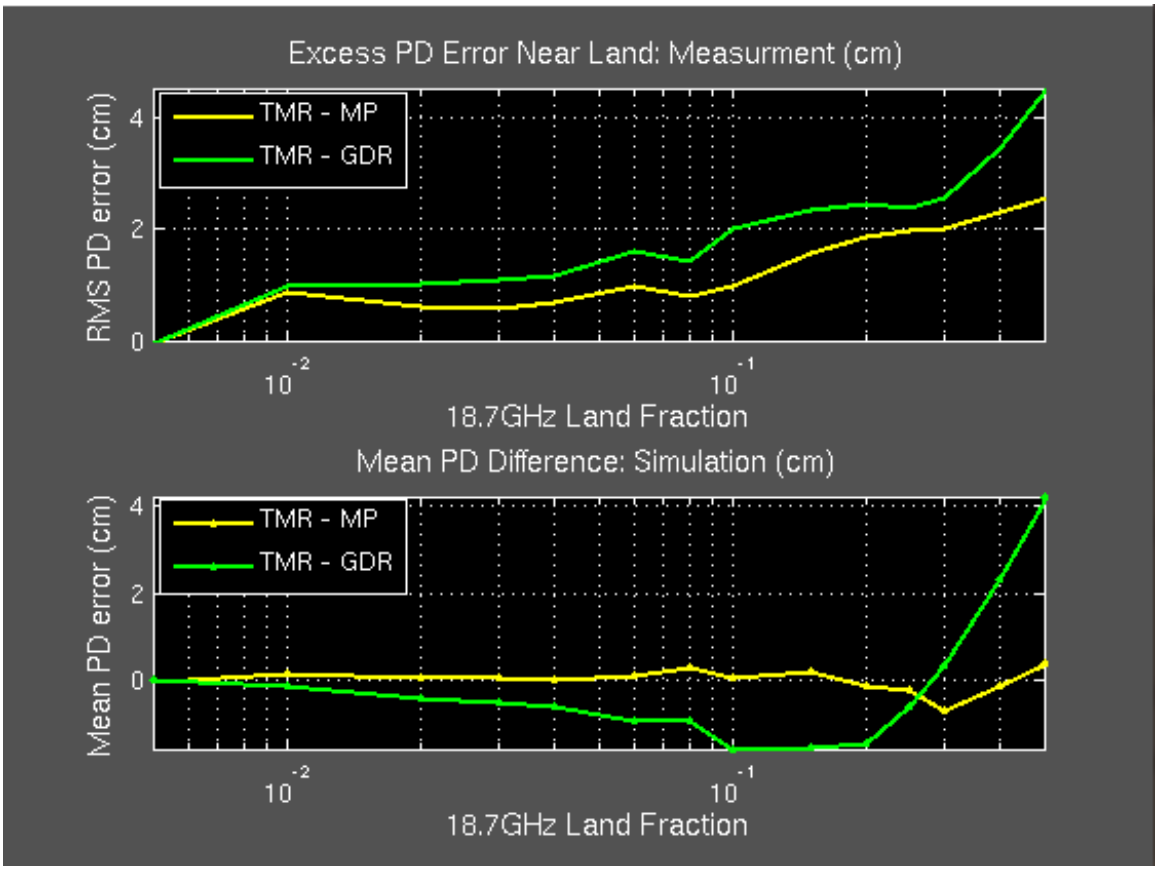

Figure 11: ***The MP algorithm successfully compensates for land contamination. The figures above show the performance of the MP algorithm in terms of mean difference and RMS error with respect to MERRA. As observed, the GDR algorithm retrieved PDs have a characteristic dip as the land fraction increases. This is due to an increase in the 18GHz Tb that is not offset by increase in the higher frequency Tbs. The mixed pixel algorithm clearly has lower mean difference and RMS error compared to the GDR algorithm.***

2.4 Ocean Tide Corrections

The ocean tide correction applied to v6.0 SSH is GOT5.6D, a variant of the Goddard Ocean Tide GOT5; a new solution for the amplitudes and phases of the daily and sub-daily global ocean tides, based on decades of radar altimetry from multiple satellite missions. Over the main part of the deep ocean, between latitudes ±66° , the solution rests primarily with the series of five satellites Topex/Poseidon, Jason-1, Jason-2, Jason-3, and Sentinel-6A Michael Freilich (Figure 12), but in

shallow seas and in polar latitudes other satellite altimeters were also used (Table 3). The tidal analysis of these data was done relative to a prior model, which for the most part was the Finite Element Solution FES2014 of Lyard et al. (2021), with some minor patches. The GOT5 solutions were thus starting with a very good global model, and the obtained results benefit greatly from that. A NASA Technical Memorandum (Ray, 2025) documents the data processing details underlying the GOT5 tides. There are several variants of GOT5, arising not only from (experimental) refinements in processing algorithms but also from different approaches to handling the problem of atmospheric loading; a special variant, GOT5.6D, was designed to be used in conjunction with the current version of the Dynamic Atmosphere Correction by attempting to overcome inadequacies in adopted models of atmospheric tides.

Table 3: Solution domains used to construct GOT5 (Table 2 from Ray, 2025).

Domain	Latitude extent	Satellites	Time span	# days
Main	±66°	Jason, S-6	2002–2023	7924
		Interleaved T/P-J	2002–2023	2961
		GFO	2000–2008	2459
		Envisat, SARAL	2002–2016	4280
		Sentinel-3A	2016–2023	2847
		Sentinel-3B	2018–2023	1860
Arctic	60°–90°N	CryoSat-2	2010–2021	3933
		GFO	2000–2008	2474
		Envisat	2002–2012	3502
		SARAL	2013–2022	3445
Antarctic	79°–60°S	CryoSat-2	2010–2021	3933
		GFO	2000–2008	2401
		Envisat	2002–2012	3502
		SARAL	2013–2022	3447
Ice shelves	86°–65°S	CryoSat-2	2010–2022	4285

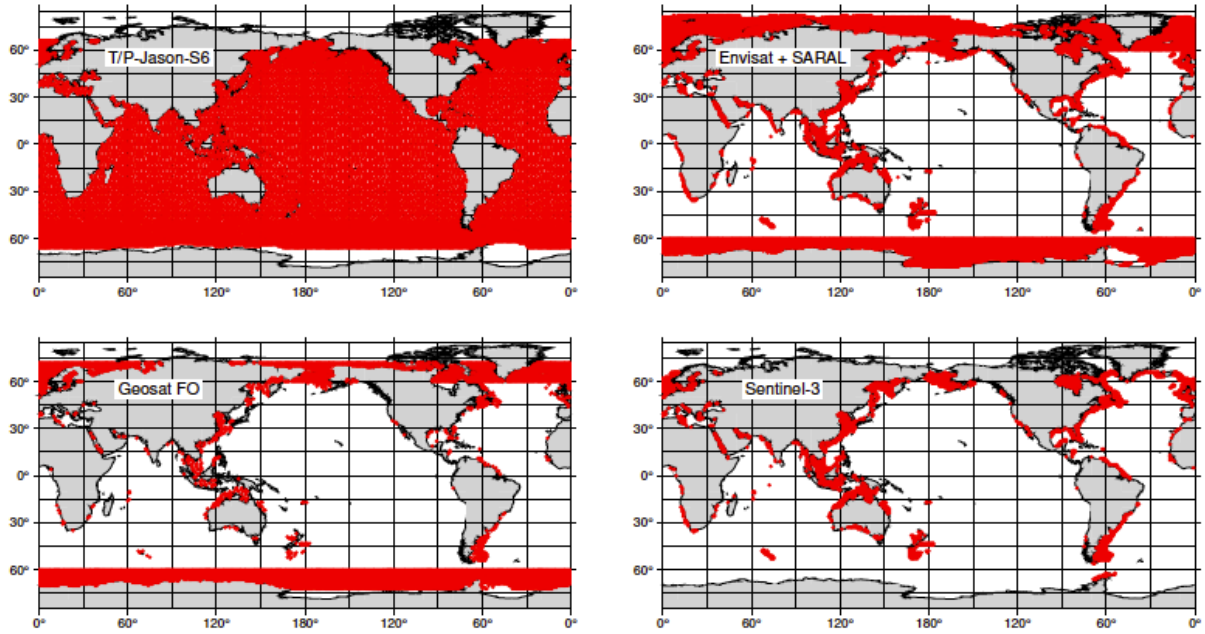

Figure 12: ***Ocean locations where altimeter data from each satellite series was used in development of GOT5. ERS-2 data were also used wherever Envisat data were (Figure 2 from Ray, 2025).***

The model for long-period ocean tides is described by Ray & Erofeeva (2014). It is a hydrodynamic solution of the long-period tidal equations, formally unconstrained by observations but fine-tuned to agree with measurements of the fortnightly Mf tide, including measurements of Mf polar motion and length of day. Five dynamic constituents are given explicitly (Sa, Ssa, Mm, Mf, and Mt, with periods from 1 year to 9 days). The prediction software automatically infers five additional constituents, and it applies standard nodal adjustments to all lunar constituents. A final constituent is included for the node tide (period 18.6 y), which takes a (self-consistent) equilibrium form. In Version 5.0 the model for the M2 internal tide is derived empirically from satellite data without reliance or knowledge of wave dynamics or ocean stratification as described by Ray and Zaron (2016). In Version 5.2 and v6.0 the revised internal tide model takes into account M2, S2, K1, and O1 tidal frequencies (Zaron, 2019).

2.5 Pole Tide Correction

Version 5.0 was first to implement a revised pole tide correction (Desai et al., 2015) that replaced the earlier model contained in the T/P and Jason GDRs. The two primary revisions to the earlier model include 1) "upgrading to a self-consistent equilibrium model for the displacement of the ocean surface relative to the Earth's crust and explicitly modeling the load pole tide with respect to the CM", and 2) "that pole tide displacements for altimetry be computed from residual polar motion with respect to a drifting mean pole, with the rate determined from almost 80 years of observations (Argus and Gross, 2004)". The impact on global mean sea level estimates is negligible due to geographical cancellation of signal. Impact on regional sea level estimates range from ±0.25 mm/y (Figure 13). Version 6.0 employs the current GDR_F pole tide correction

(version 2.2) based on a further revision to the mean pole position determination (Ries and Desai, 2107).

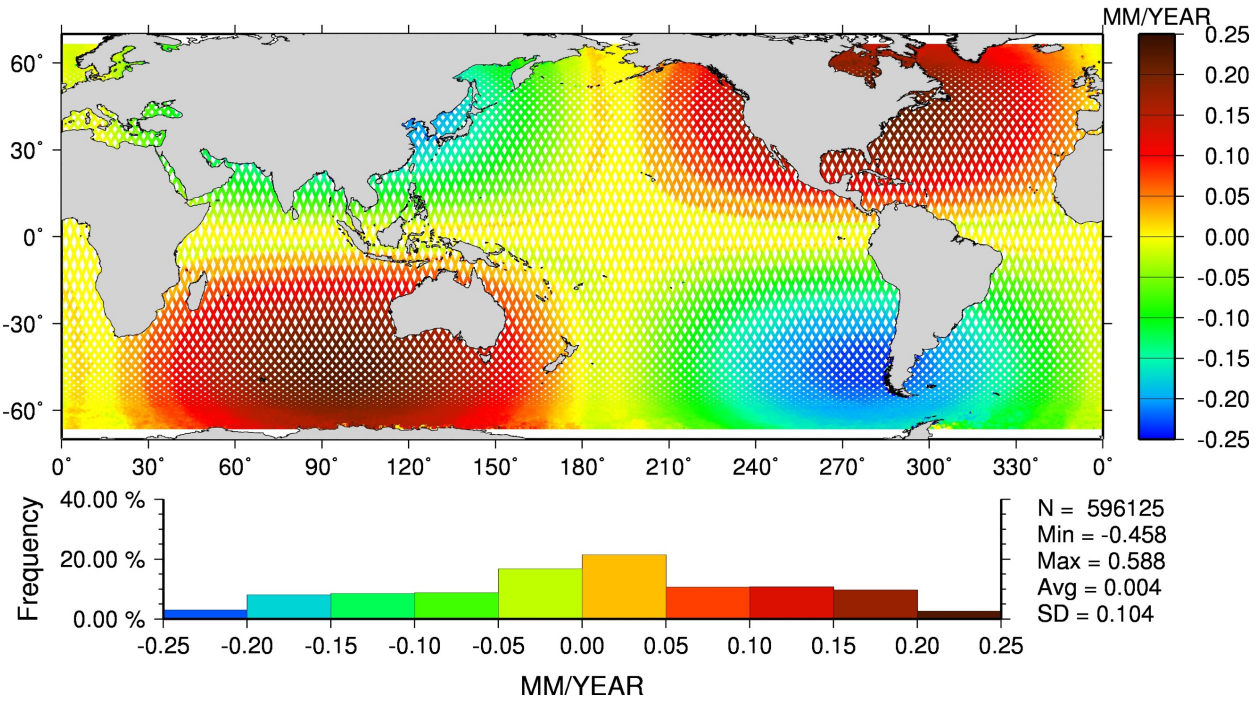

Figure 13: ***Regional linear trends of pole tide differences between revised model (Desai, et al., 2015) and previous model contained in mission GDRs. The impact on regional sea level is at the level of +/- 0.25 mm/y.***

2.6 Mean Sea Surface

The DTU15 mean sea surface (Andersen, 2015.) replaced the DTU13 surface as the reference for the SSH anomalies, and for the generation of the cross-track gradient correction derived from the regional slopes at each geo-referenced location. Additional altimetry derived from a 22+ year record and the inclusion of the Jason-1 geodetic mission data and CryoSat-2 data are incorporated in the generation of the DTU15 surface. Revised cross-track slopes based on the DTU15 MSS are shown in Figure 14.

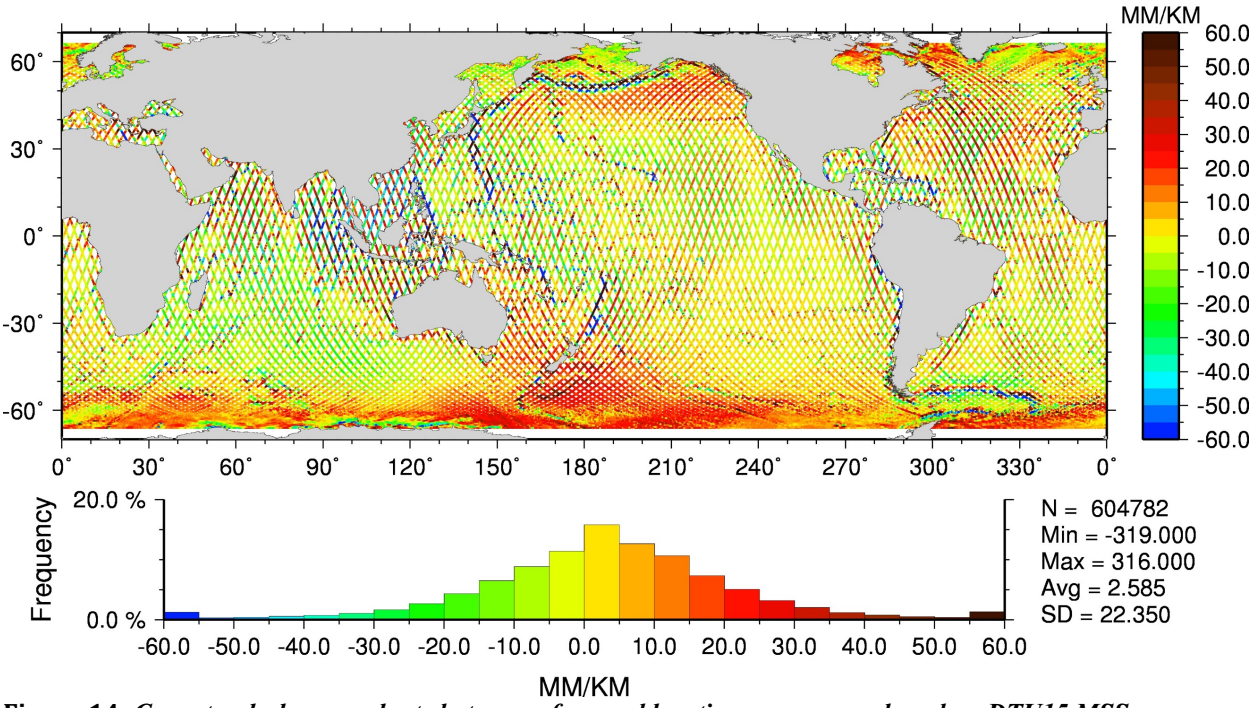

Figure 14: ***Cross-track slopes evaluated at geo-referenced locations over ocean based on DTU15 MSS.***

3.0 Inter-mission biases

3.1 Verification Phase Results

A critical component to providing credible mean sea level estimates from integrated multiple altimeter missions is the accurate determination of inter-mission biases. The verification campaigns during the roughly first 6 months of the Jason-1, 2, and 3 missions provided essential near-simultaneous altimeter observations that would enable the seamless transition from T/P to Jason-1 to Jason-2 to Jason-3 to Sentinel-6a.

Figures 15 through 18 show the estimated global mean bias between TOPEX/Jason-1, Jason-1/Jason-2, Jason-2/Jason-3, and Jason-3/Sentinel-6a respectively derived from the averaged per cycle mean variations of the SSH collinear differences of the near-coincident measurements over the time period of the verification phase(s). All pertinent range and geophysical corrections are applied in order to identify and isolate any regional residual differences/errors attributed to any remaining unavoidable inter-mission inconsistencies. Each figure shows some expected regional variance in the estimate of the global mean bias estimate, though each estimate has a very normalized distribution of SSH mean residuals with a standard deviation not exceeding 2 mm.

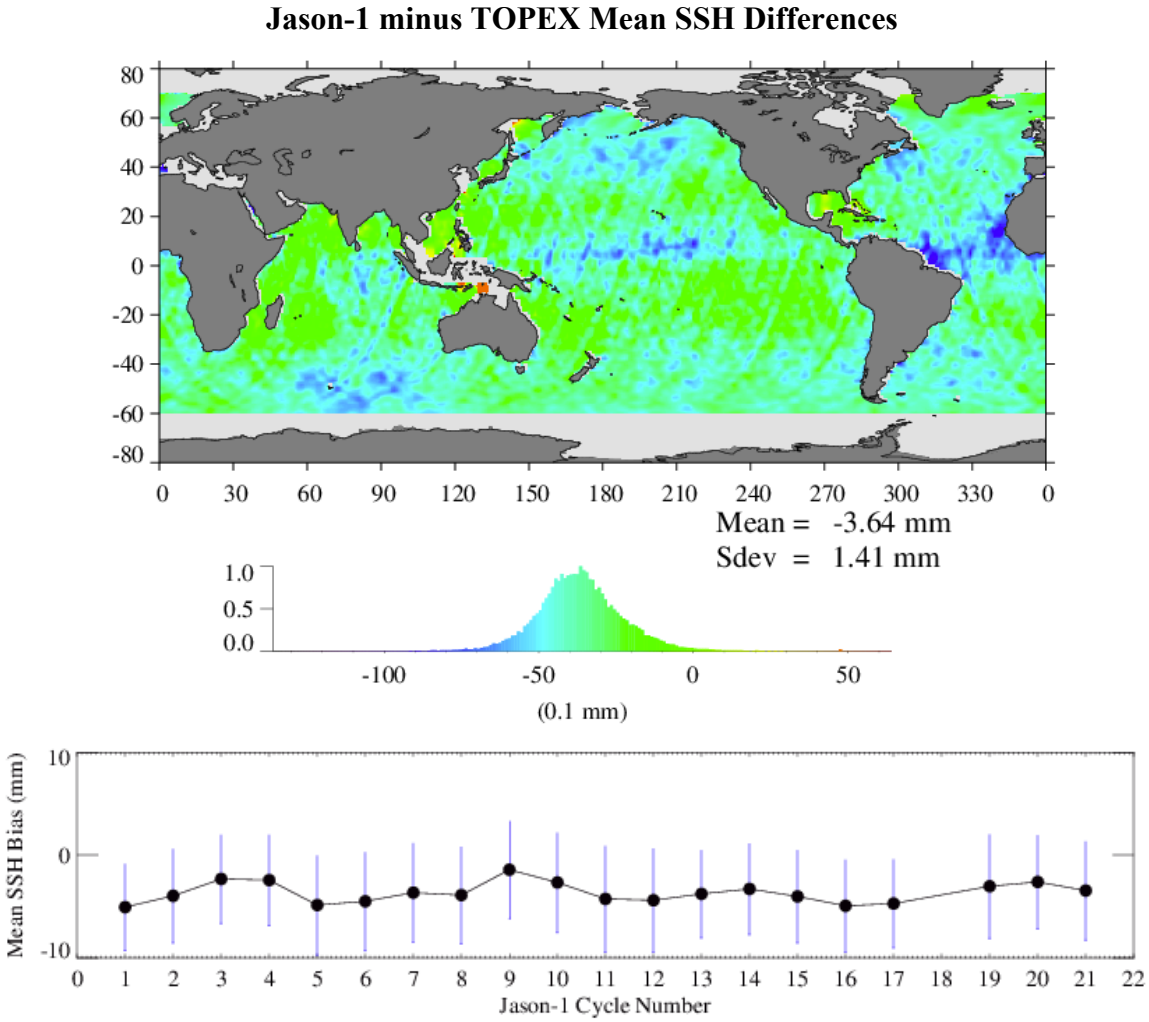

Figure 15: v6.0 Jason-1 minus TOPEX (Alt B) inter-mission bias is estimated from averaged per cycle SSH collinear residuals during the Jason-1 verification phase. Color scale is +/- 1cm about estimated global mean.

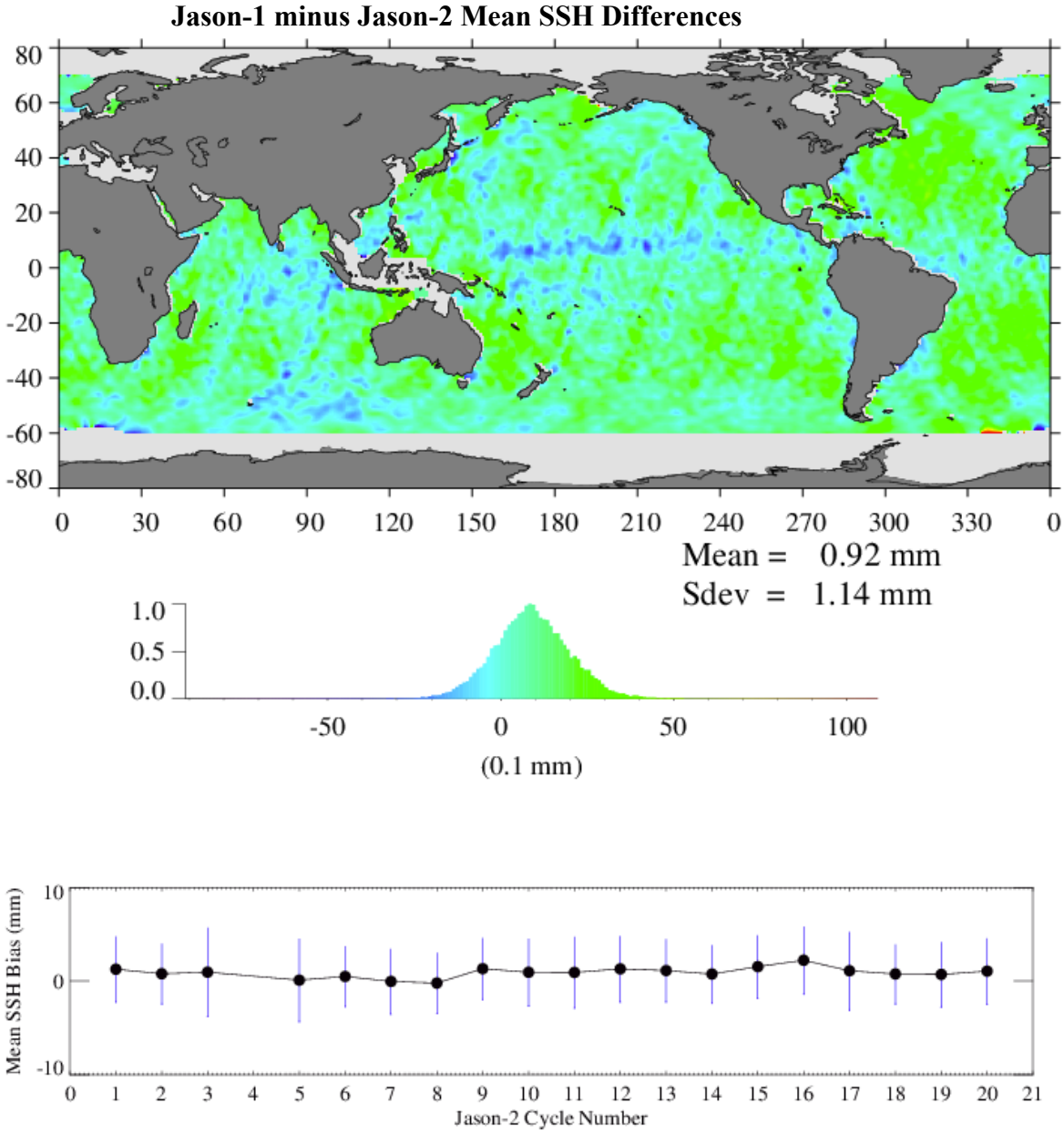

Figure 16: ***v6.0 Jason-1 minus Jason-2 inter-mission bias is estimated from averaged per cycle SSH collinear residuals during Jason-2 verification phase. Color scale is +/- 1cm about estimated global mean.***

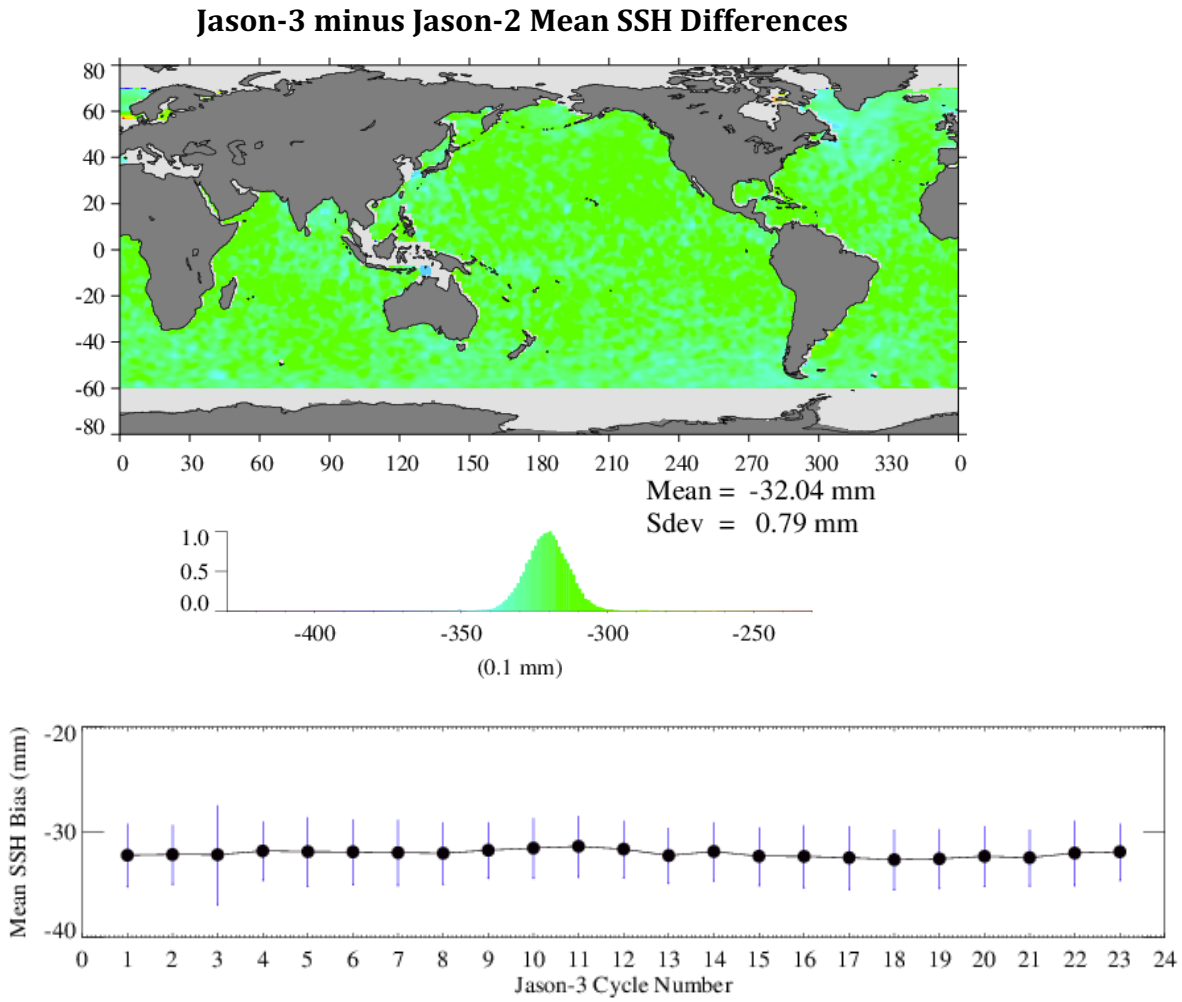

Figure 17: ***v6.0 Jason-3 minus Jason-2 inter-mission bias is estimated from averaged per cycle SSH collinear residuals during Jason-3 verification phase. Color scale is +/- 1cm about estimated global mean.***

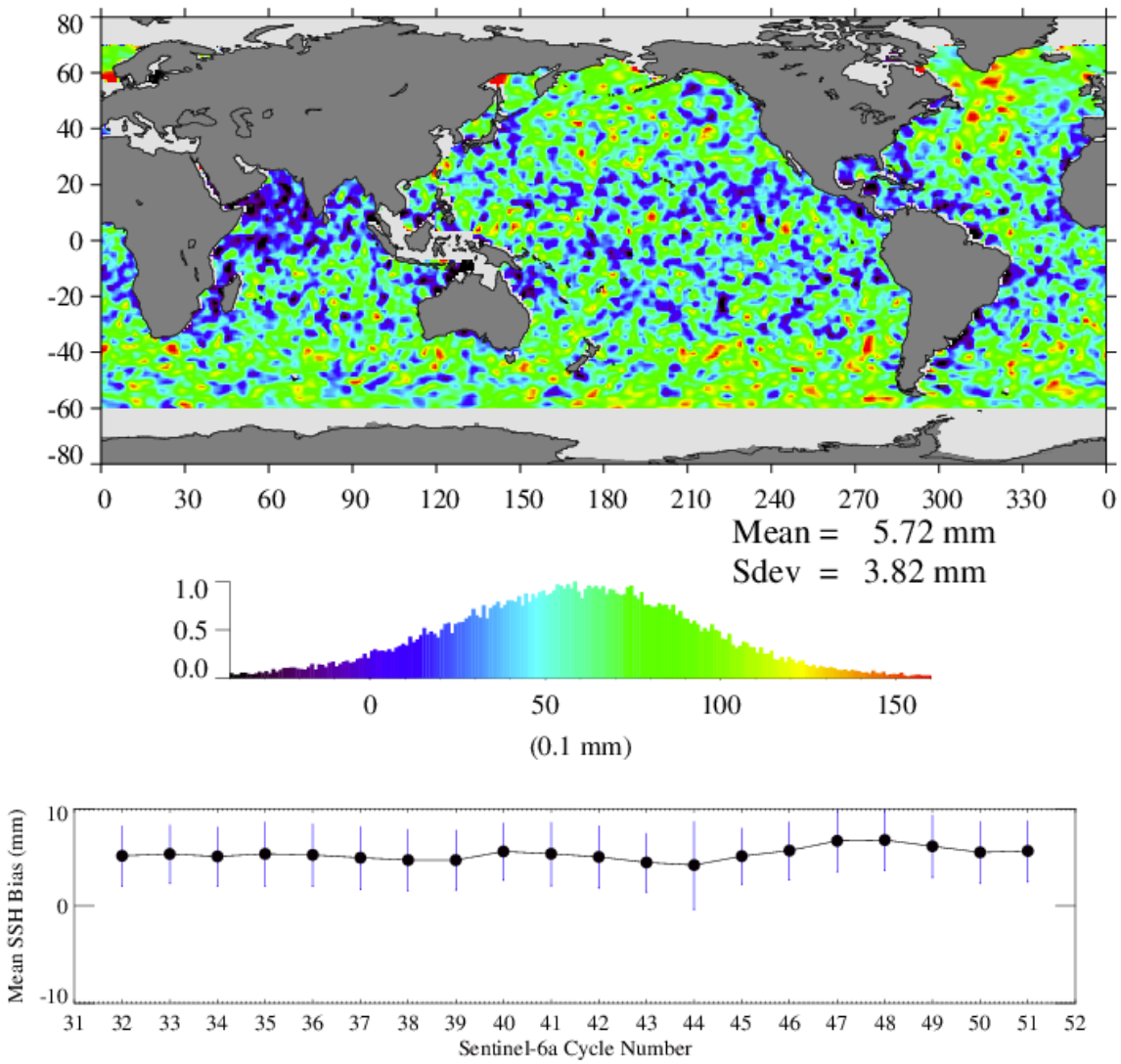

Figure 18: ***v6.0 Sentinel-6a minus Jason-3 inter-mission bias is estimated from averaged per cycle SSH collinear residuals during Sentinel-6 verification phase (cycles 32-51). Color scale is +/- 1cm about estimated global mean.***

3.2 Tide Gauge Validations

Validation procedures are regularly performed by Prof. Gary Mitchum by comparing altimeter derived SSH variations to height variations measured from a global network of tide gauges (Mitchum, 2000). From the beginning of the TOPEX/Poseidon (T/P) mission, methods to estimate altimeter drift from comparisons with the global tide gauge network have continuously evolved, (for example, as the SSH time series approached two decades, questions about the handling of long period tides, particularly the Msf and Mf components, were raised and we adapted our methods appropriately) first in a research mode with NASA funding (primarily the T/P and OST SWTs and later from MEaSUREs), and later becoming general and operationally-oriented.

Validation results shown here are based on the current near-global network of 64 sites (Figure 19). The largest uncertainty in estimated rates derived from the gauges arises from land motion at the sites. Vertical land motion corrections based on the latest ULR6 (University of La Rochelle Consortium) GPS velocity fields (Santamaría-Gómez et al., 2012, Wöppelmann et al., 2009) have been implemented.

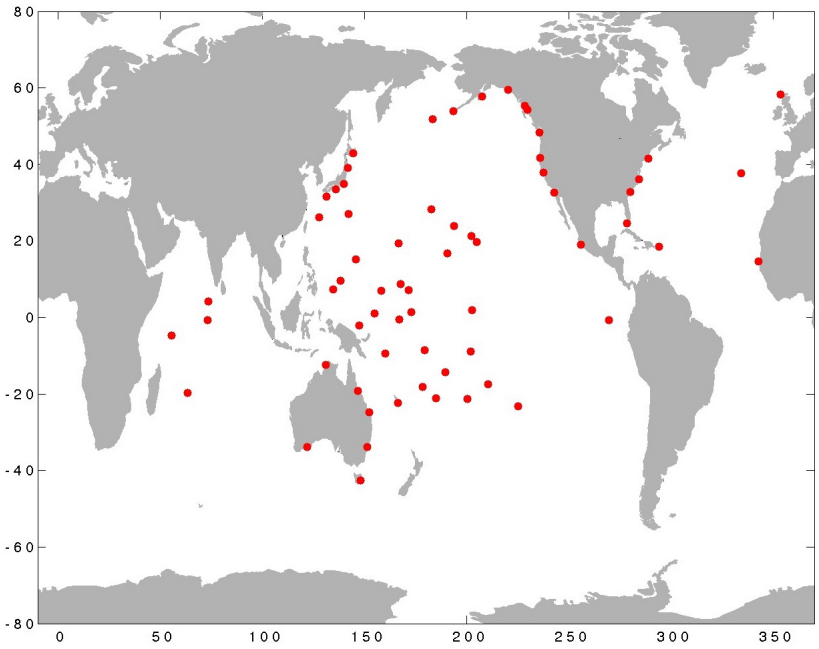

Figure 19: ***Current network of 64-tide gauge sites (red dots).***

The tide gauge validation analysis tools currently in place evaluates and monitors within-mission stability and provides an assessment of inter-mission bias estimates (Ray et al., 2010, Leuliette and Scharoo, 2010, Nerem, et al., 2010, 2018). As shown in figures 15 through 18, TOPEX/Jason-1, Jason-1/Jason-2 (J1/J2), Jason-2/Jason-3, and Jason-3/Sentinel-6a inter-mission biases can be evaluated globally by direct SSH collinear differencing benefiting from the dedicated verification phases. Note the inter-mission biases listed in Table 1 were derived after additional editing of anomalous revolutions from the first iteration shown. The TOPEX Side A (Launch – February 10, 1999) and Side B altimeters are treated as if separate missions as is noted in the independent evaluation of the sea state bias for each altimeter. There is no Side A/B coincident overlapping data available thus we are reliant on the tide gauge network to estimate this particular "inter-

mission" bias. The TOPEX Side A calibration data experienced a "jump" on April 1, 1996, thus users were "advised to treat data from Side A1 (Launch – April 1, 1996) Side A2 (April 1, 1996 – February10, 1999) as two independent time series" (TOPEX GDR_F Handbook). Figure 20 shows the unadjusted Side A1 and A2 per cycle mean altimeter minus tide-gauge variations. The TOPEX/Poseidon-1 biases are estimated by computing the mean of the adjusted TOPEX – Poseidon-1 open-ocean collinear SSH residuals via adjacent T/P cycles (figure 21).

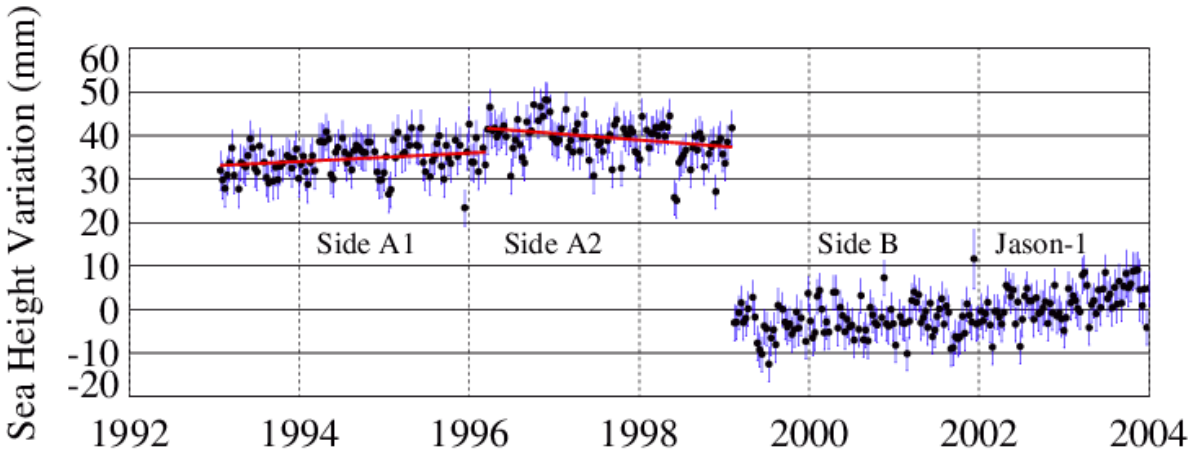

Figure 20: ***Estimate of v6.0 TOPEX Side A/B bias is derived from per cycle mean comparisons of altimeter SSH variations with height variations from 64-site tide gauge network. The TOPEX Side B data is adjusted from collinear residuals during the Jason-1 verification phase (see Figure 11). Separate bias adjustments are estimated for TOPEX Side A1 and A2 from mean per cycle altimeter SSH minus tide gauge height variations.***

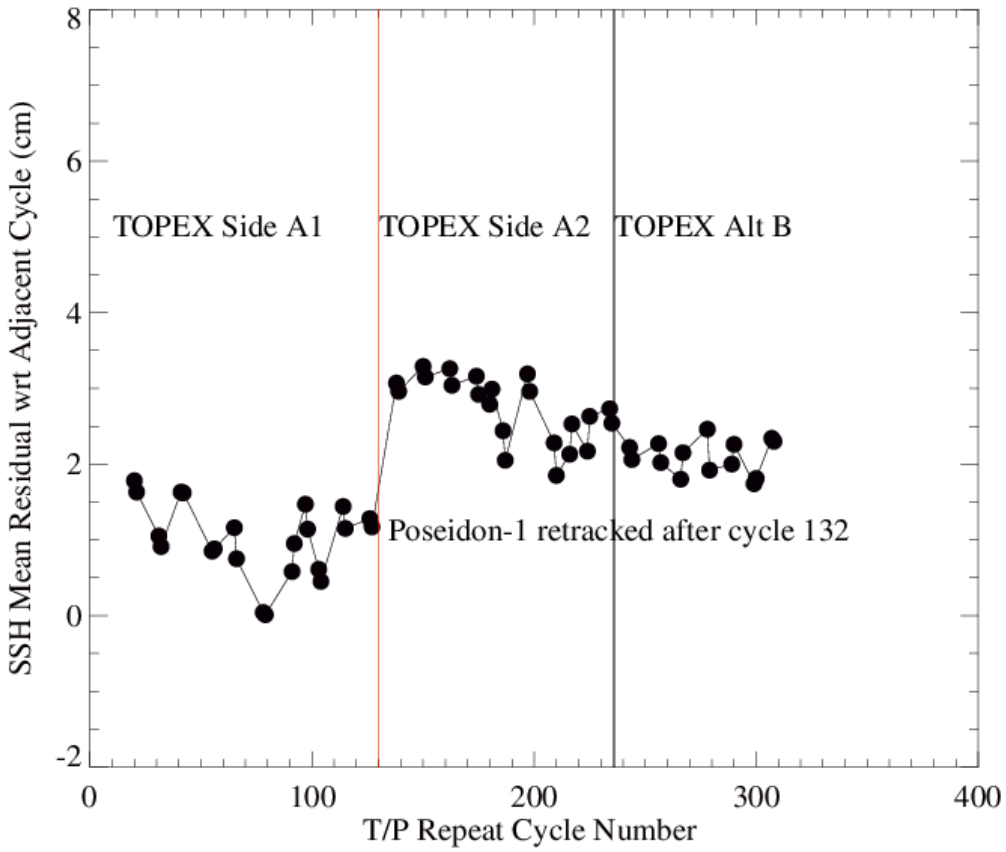

Figure 21: ***Poseidon-1 bias with respect to adjusted v6.0 TOPEX is estimated via mean collinear TOPEX minus Poseidon-1 SSH residuals. Before cycle 132, Poseidon-1 data is not retracked.***

To assess the inter-mission consistency and stability of the entire 32+ year time series, the TOPEX A/B bias, and the adjustment biases to Jason-1 and Jason-3 that were derived from their verification campaign SSH collinear residuals are applied, and compared against a high-fidelity 64-site tide-gauge network as a "single mission" time series. These tide gauge comparisons provided in Figure 22 show v5.2 and v6.0 per cycle mean differences to be predominantly within a ± 1.0 cm envelope, with v6.0 having an overall estimated "drift" rate less than 0.1 mm/y +/- 0.4 mm/y with a standard deviation of the mean altimeter minus tide gauge differences of less than 4 mm.

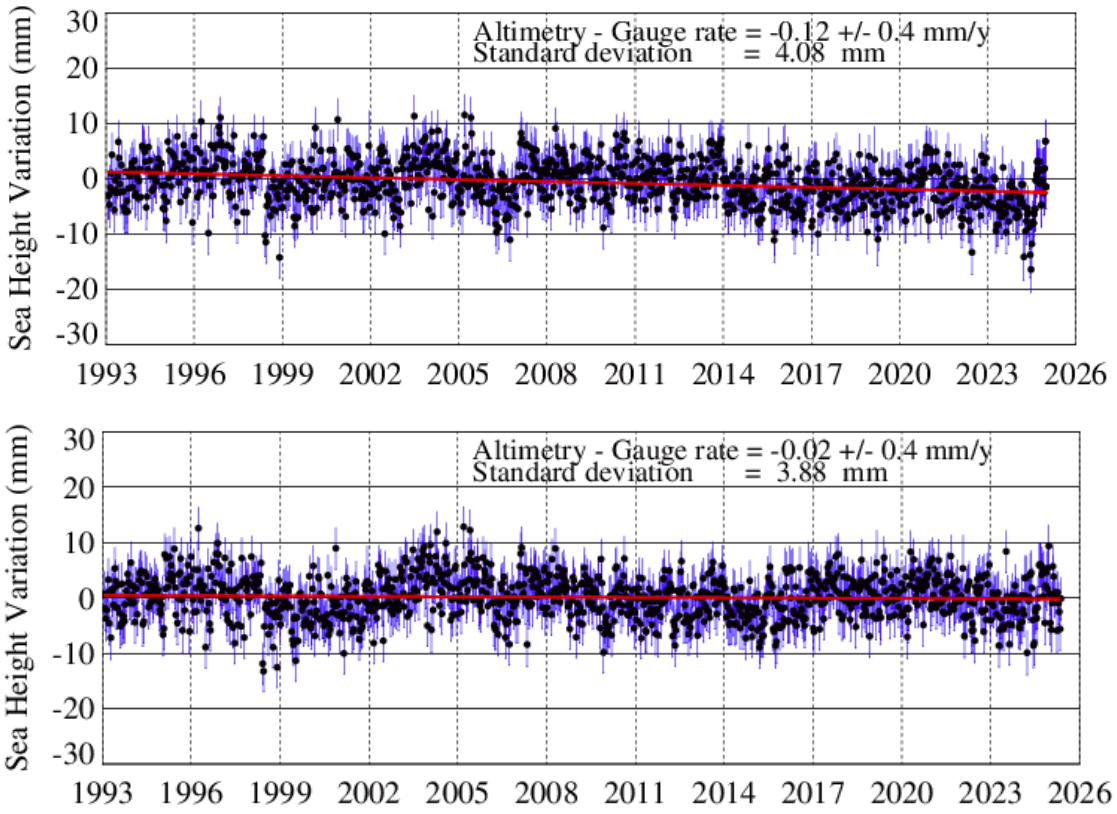

Figure 22: ***Resultant per cycle comparisons of altimeter derived v5.2 (top panel) and v6.0 (bottom panel) SSH variations with height variations from 64-site tide gauge network after application of inter-mission biases to form a single adjusted SSH Climate Data Record.***

4.0 Estimation of Global and Regional Mean Sea Level

Global and regional mean sea level variations derived from the v6.0 product is shown in Figures 23 through 25 below. Details of the derivation of the sea level estimates are provided in Beckley et al., 2007 and 2010. The examples below do have the glacial isostatic adjustment (GIA; Peltier 2009) applied; annual and semi-annual signals are intact in Figure 19, and have been removed in Figures 20 and 21. The edit strategy employed based on the quality flag word bits edited observations where any one of bits 4-6, 9-14 where set to 1, or bits 7 and 8 both set to 1 (see Appendix). The GMSL estimates have a coastal mask editing observations that were within 10 km to land and less than 20 meters in depth. The regional sea level map (Figure 25) contains coastal sea level rates.

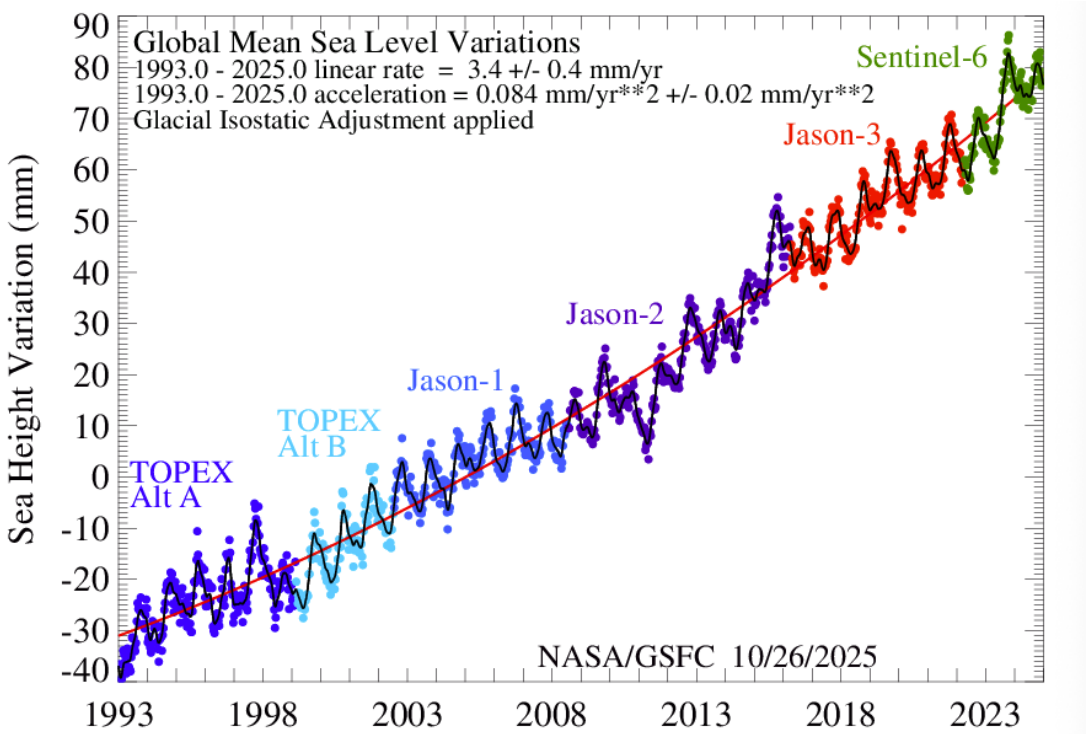

Figure 23: ***Global mean sea level is estimated at 3.4 ± 0.4 mm/yr (GIA applied, seasonal signals retained) based on SSH variations with respect to 20-year TOPEX/Jason mean profile. Sea surface height variations are based on cycles 11-1189 (1993.0 – 2025.0) of NASA-SSH v6.0 SSH anomaly product. Black line denotes SSH variation after application of 60-day Hanning filter. Red line is a quadratic fit of the filtered SSH variations indicating an acceleration of +0.084 mm/yr**2 ± 0.02 mm/yr**2.***

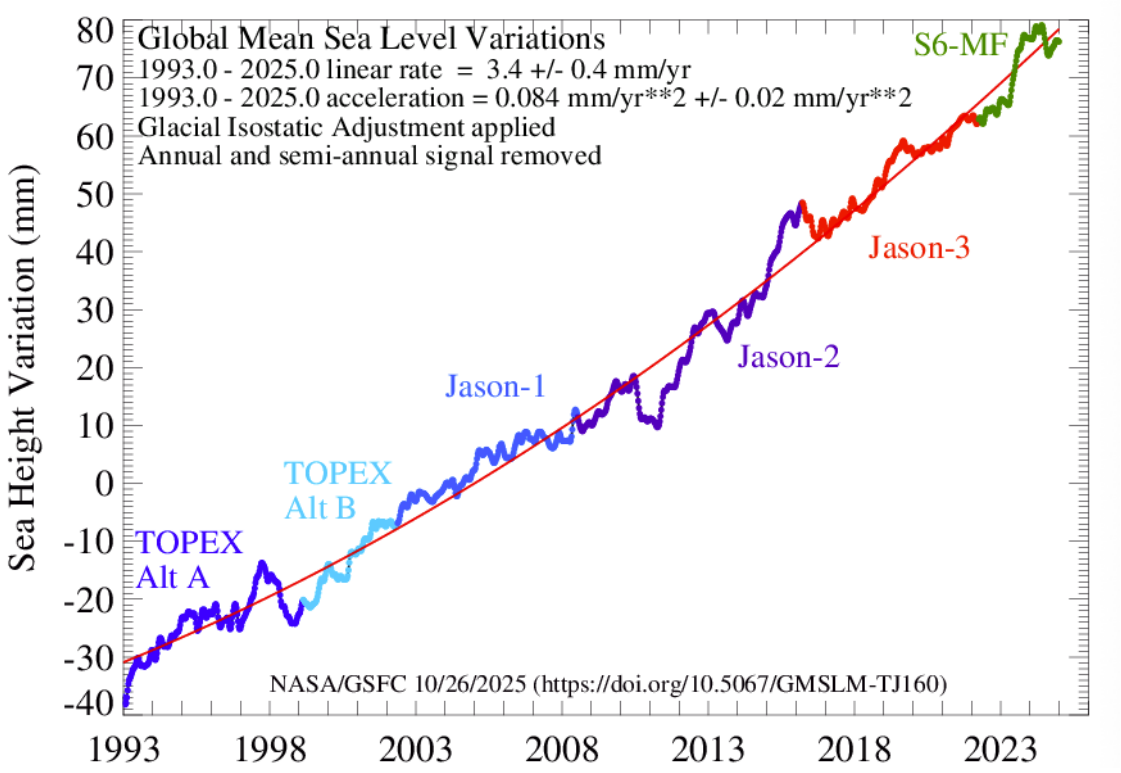

Figure 24: ***Global mean sea level variations estimated as in Figure 23 with annual and semi-annual signal removed.***

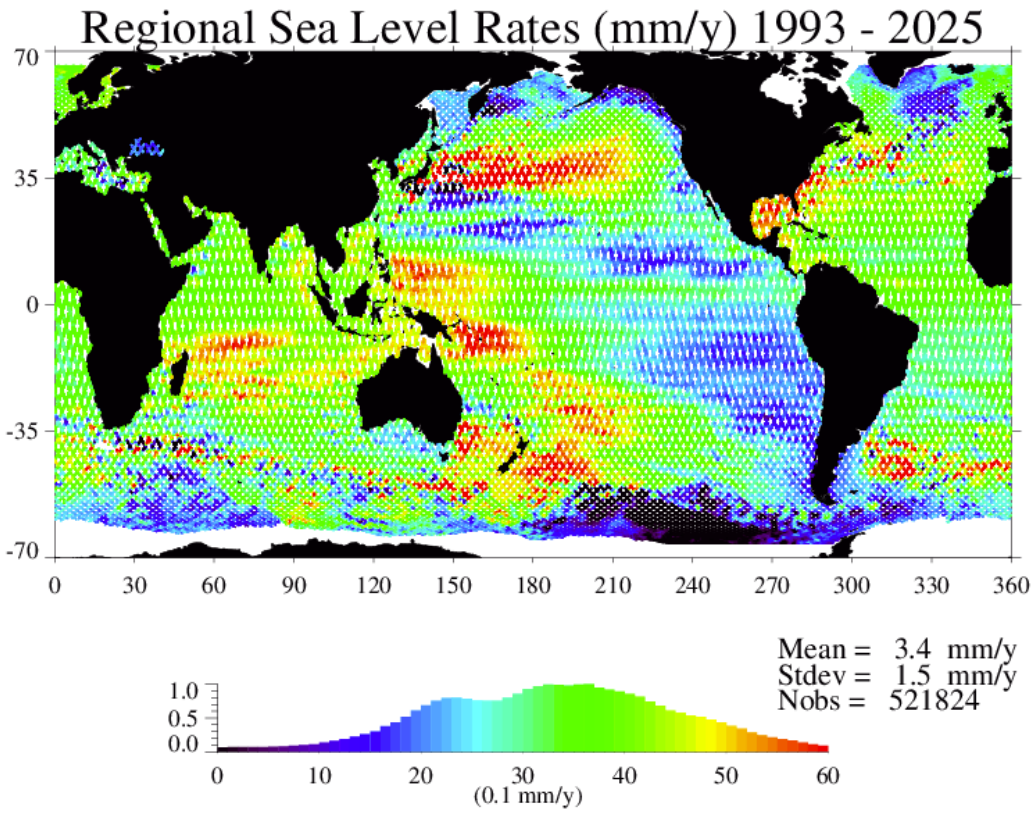

Figure 25: ***Regional mean sea level variations (GIA applied) at each geo-referenced location are based on cycles 11-1189 (1993.0-2025.0) of the NASA-SSH v6.0 SSH anomaly product.***

5.0 References

Altamimi, Z., P. Rebischung, L. Metivier, and C. Xavier (2016), ITRF2014: A new release of the International Terrestrial Reference Frame modeling nonlinear station motions, *J. Geophys. Res. Solid Earth*, 121, doi:10.1002/2016JB013098.

Altamimi Z., Rebischung P., Collilieux X. et al. (2023) "ITRF2020: an augmented reference frame refining the modeling of nonlinear station motions.", J. *Geodesy, 97,* 47, doi:10.1007/s00190-023-01738-w.

Andersen, O. B., G. Piccioni, L. Stenseng, and P. Knudsen, The DTU15 Mean Sea Surface and Mean Dynamic Topography-focusing on Arctic issues and development., 2015 Ocean Surface Topography Science Team Meeting, Reston, VA, USA.

Argus DF, Gross RS (2004) An estimate of motion between the spin axis and the hotspots over the past century. *Geophys Res Lett* 31. doi:10.1029/2004GL019657

Beckley, B.D., N.P. Zelensky, S.B. Luthcke, and P.S. Callahan. 2004. Towards a seamless transition from TOPEX/Poseidon to Jason-1. *Marine Geodesy,* 27, 373-384.

Beckley, B.D., F.G. Lemoine, S.B. Luthcke, R.D. Ray, and N.P. Zelensky. 2007. A reassessment of TOPEX and Jason-1 altimetry based on revised reference frame and orbits. *Geophys. Res. Lett.*, 34, L14608, doi:10.1029/2007GL030002.

Beckley, B.D., N.P. Zelensky, S.A. Holmes, F.G. Lemoine, R.D. Ray, G.T. Mitchum, S. Desai, S.T. Brown, Assessment of the Jason-2 Extension to the TOPEX/Poseidon, Jason-1 Sea-Surface Height Time Series for Global Mean Sea Level Monitoring, *Marine Geodesy*, 33(S1): 447-471, 2010, Supplemental Issue on OSTM/Jason-2 calibration/validation, Vol. 1, DOI: 10.1080/01490419.2010.491029.

Beckley, B. D., Callahan, P. S., Hancock, D. W., Mitchum, G. T., & Ray, R. D. (2017). On the "cal-mode" correction to TOPEX satellite altimetry and its effect on the global mean sea level time series. *Journal of Geophysical Research: Oceans*, 122. https://doi.org/10.1002/2017JC013090.

Benada, J. R., 1997. "*PO.DAAC Merged GDR (TOPEX/POSEIDON) Generation B User's Handbook"*, Version 2.0, JPL D-11007.

Brenner, A. C., C. J. Koblinsky, and B. D. Beckley. 1990. A Preliminary Estimate of Geoid-Induced Variations in Repeat Orbit Satellite Altimeter Observations. *J. Geophys. Res.,* 95(C3), 3033- 3040.

Brown, S., S. Desai, N. Lahaye, The End-of-Mission Climate Quality Calibration for the JMR, 2014 Ocean Surface Topography Science Team Meeting, Konstanz, Germany, http://meetings.aviso.altimetry.fr/fileadmin/user_upload/tx_ausyclsseminar/files/28Ball1400-3_OSTST_14_JMR_calibration_Brown.pdf

Brown, S., S. Desai, Chae, C. (2023) Progress on the wet path delay correction: Historical, Current, and Future, 2023 OSTST meeting, San Juan, Puerto Rico, Nov., 2023.

Cadier, E., G. Bracher, B. Courcol, C. Kocha, P. Prandi, M. Pujol, C. Maraldi, F. Bignalet-Cazalet, (2024) Comparison of Jason-3 and Sentinel-6MF observations in the equatorial band: Was TOPEX right from the start? 30-Years of Progress in Radar Altimetry Symposium, Monpelier, France.

Carrère, L., and F. Lyard. 2003. Modelling the barotropic response of the global ocean to atmospheric wind and pressure forcing. *Geophys. Res. Lett.,* 30(6), art. 1275, DOI:10.1029/2002GL016473.

Conrad A., Desai S., Haines B., Axelrad P. (2023). "Extending the GPS IIIA antenna calibration for precise orbit determination of low Earth orbit satellites", *J. Geodesy, 97(35),* doi:10.1007/s00190-023-01718-0.

Conrad A., Desai S., Haines B., Forster L. (2024). "GPS-based precise orbit determination of the Sentinel-6 MF and Jason-3 Missons", Presentation at the 30 years in Radar Altimetry Symposium, September 2–7, 2024, Montpelier, France, https://www.altimetry2024.org/programme

Chambers, D.P., S.A. Hayes, J.C. Ries, T.J. Urban. 2003. New TOPEX Sea State Bias Models and their Effect on Global Mean Sea Level. *J. Geophys Res*., 108, 3305.

Desai, S., J. Wahr, B. Beckley, Revisiting the pole tide for and from satellite altimetry, *Journal of Geodesy*, 89(8), 747-842, 2015. DOI 10.1007/s00190-015-0848-7

Jason-3 Products Handbook, CNES: SALP-MU-M-OP-16118-CN, September 21, 2020.

Kummerow, C. and W. Berg, A Fundamental Climate Data Record SSMI and SSMIS Science Data Stewardship, 2010 Workshop on Climate Data Records from Satellites, Silver Spring, MD, March 22-24, 2010. http://www.orbit.nesdis.noaa.gov/star/documents/meetings/CDR2010/talks/DayOne/Kummerow_C.pdf

Lemoine, F.G., N.P. Zelensky, B.D. Beckley**,** G.T. Mitchum, X. Yang, J.B. Nicholas (2025), Precise orbit determination for TOPEX/Poseidon, Jasons 1,2,3 and Sentinel-6A and the std2400 series of orbits, *Adv. Space Research* (in review).

Lemoine, F.G., N.P. Zelensky, D.S. Chinn, D.E. Pavlis, D.D. Rowlands, B.D. Beckley**,** S.B. Luthcke, P. Willis, M. Ziebart, A. Sibthorpe, J. Boy, V. Luceri, Towards development of a consistent orbit series for TOPEX, Jason-1, and Jason-2, *Adv. Space Research*, 46 (2010) 1513-1540, doi: 10.1016/j.asr.2010.05.007

Lemoine, F.G., N.P. Zelensky, D.S. Chinn, B.D. Beckley, D.D. Rowlands, D.E. Pavlis (2015) A new time series of orbits (std1504) for TOPEX/Poseidon. Jason-1, and Jason-2 (OSTM), Ocean Surface Topography Science Team Meeting, Reston, VA. http://meetings.aviso.altimetry.fr/?id=95&nocache=1&tx_ausyclsseminar_pi2%5bobjAbstract%5d=1716&nocache=1&useCacheHash=1&cHash=1

Leuliette, E.W., and R. Scharroo, Integrating Jason-2 into a Multiple-Altimeter Climate Data Record, *Marine Geodesy*, 33(S1) : 504-517, 2010, Supplemental Issue on OSTM/Jason-2 calibration/validation, Vol. 1, DOI : 10.1080/01490419.2010.487795.

Lyard, F., Allain, D., Cancet, M., Carrère, L., & Picot, N. (2021). FES2014 global ocean tides atlas: design and performance. Ocean Science, 17, 615–649. doi: 10.5194/os-17-615-2021

Mitchum, G.T. 2000. An improved calibration of satellite altimetric heights using tide gauge sea levels with adjustment for land motion. *Marine Geodesy*, 23, 145-166.

Misra, S. and S. Brown, Application of a Mixed-Pixel Algorithm to TOPEX for Coastal Wet Tropospheric Delay Retrieval, 2011 Coastal Altimetry Workshop poster presentation.

Nerem, R.S., D.P. Chambers, C. Choe, G.T. Mitchum, Estimating Mean Sea Level Change from the TOPEX and Jason Altimeter Missions, *Marine Geodesy*, 33(S1): 435-446, 2010, Supplemental Issue on OSTM/Jason-2 calibration/validation, Vol. 1, DOI: 10.1080/01490419.2010.491031.

Nerem, R. S., B.D. Beckley, J. T. Fasullo, B.D. Hamlington, D. Masters, and G. T. Mitchum, 2018. "Climate-change–driven accelerated sea-level rise detected in the altimeter era." *Proceedings of the National Academy of Sciences*, 201717312 [10.1073/pnas.1717312115]

OSTM/Jason-2 products handbook, CNES: SALP-MU-OP-15815-CN, Issue : 2 rev 0, April 15, 2025.

Picot, N., et al., 2016, Jason-1 Products Handbook, References: CNES : SALP-MU-M5-OP-13184-CN JPL: JPL D-21352 Issue: 5 rev 1 Date: April 4th, 2016

Peltier, W. R., 2009. Closure of the budget of global sea level rise over the GRACE era: The importance and magnitude of the required corrections for global glacial isostatic adjustment, Quat. Sci. Rev. 17–18:1658–1674, doi:10.1016/j.quascirev.2009.04.004.

Picot, N., K. Case, S. Desai, and P. Vincent. 2008. *AVISO and PODAAC User Handbook. IGDR and GDR Jason Products, Edition 4.0*. SMM-MU-M5-OP-13184-CN (**AVISO**), JPL D-21352 (**PODAAC**).

Picot, N., et al., 2016, Jason-3 Products Handbook, Issue 1, revision 2, February 12, 2016, CNES : SALP-MU-M-OP-16118-CN

Ray, R.D. 1999. A global ocean tide model from TOPEX/Poseidon altimetry: GOT99.2, NASA TM-1999-209478, NASA Goddard Space Flight Center, September 1999 (Update).

Ray, R.D., B.D. Beckley, F.G. Lemoine. Vertical crustal motion derived from satellite altimetry and tide gauges, and comparisons with DORIS measurements. *Adv. Space Research*, 45 (2010) 1510-1522, doi: 10.1016/j.asr.2010.02.020

Ray, R. D. and S.Y. Erofeeva (2014), Long-period tidal variations in the length of day, *Journal of Geophysical Research: Solid Earth*, 119, 1498-1509, doi:10.1002/2013JB010830.

Ray, R. D. and E. Zaron (2016), "M2 internal tides and their observed avenumber spectra from satellite altimetry," *J. Phys. Oceanography*., 46(1), 3-22. doi:10.1175/JPO-D-15-0065.1

Ray, R.D. (2025). "Documentation for Goddard Ocean Tide Solution GOT5: Global Tides from Multimission Satellite Altimetry", NASA TM-20250002085, Goddard Space Flight Center, Greenbelt, Maryland, USA

Ries, J. C., and S. D. Desai (2017), Conventional model update for rotational deformation, Fall AGU, 2017. http://dx.doi.org/10.26153/tsw/2659.

Rudenko S, Dettmering D, Esselborn S, Schoene T, Foerste C, Lemoine J-M, Ablain M, Alexandre D, Neumayer K-H (2014) Influence of time variable geopotential models on precise orbits of altimetry satellites, global and regional mean sea level trends. *Advances in Space Research,* doi: 10.1016/j.asr.2014.03.010

Santamaría-Gómez, A., M. Gravelle, X. Collilieux, M. Guichard, B. Martín Míguez, P. Tiphaneau, and G. Wöppelmann (2012), Mitigating the effects of vertical land motion in tide gauge records using state-of-the-art GPS velocity field, *Global Planet. Change*, 98-99, 6–17.

TOPEX Ground System Science Algorithm Specification, JPL D-7075, Rev. A, Change 1; April 25, 1991.

Tran, N., Phillips, E. Bronner, and N. Picot, Impact of GDR_D standards on SSB corrections, Ocean Surface Topography Science Working Team Meeting, Venice, Italy, 2012. http://www.aviso.oceanobs.com/fileadmin/documents/OSTST/2012/oral/02_friday_28/01_instr_processing_I/01_IP1_Tran.pdf

Tran, N., S. Labroue, S. Phillips, E. Bronner, and N. Picot, Overview and Update of the Sea State Bias Corrections for the Jason-2, Jason-1, and TOPEX Missions. *Mar. Geod.* 33(S1): 348-362, 2010. DOI: 10.1080/01490419.2010.487788

Wöppelmann, G., C. Letetrel, A. Santamaria, M.-N. Bouin, X. Collilieux, Z. Altamimi, S.D.P. Williams, B. Martin Miguez, 2009. Rates of sea-level change over the past century in a geocentric reference frame. *Geophys. Res. Lett*. 36, L12607, 2009.

Zaron E. D, 2019, Baroclinic tidal sea level from exact-repeat mission altimetry. *Journal of Physical Oceanography*, 49(1) :193-210

Zelensky, N.P., F.G. Lemoine, B.D. Beckley, D.S. Chinn, D.E. Pavlis, Impact of ITRS 2014 Realizations on Altimeter Satellite Precise Orbit Determination, *Advances in Space Research,* 10.1016/j.asr.2017.07.044.

Acknowledgements

This work was performed in part at NASA's Goddard Space Flight Center, supported by NASA's Ocean Surface Topography program. A portion of this work was carried out at the Jet Propulsion Laboratory, California Institute of Technology, under contract 80NM0018D0004 with the National Aeronautics and Space Administration. We are grateful to NASA's Dr. Nadya Vinogradova-Schiffer for continuing support.